Czech Technical University in Prague
Faculty of Electrical Engineering
Department of Measurement

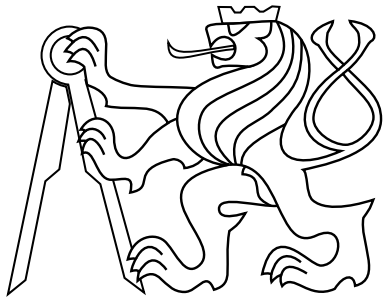

DIPLOMA THESIS

Compact Aerometric Probe

Author: Bc. Libor Urbaník
Supervisor: doc. Ing. Pavel Pačes, Ph.D.

January 2017

ČESKÉ VYSOKÉ UČENÍ TECHNICKÉ V PRAZE
Fakulta elektrotechnická
Katedra měření

Akademický rok **2015-16**

ZADÁNÍ DIPLOMOVÉ PRÁCE

Student:	**Bc. Libor Urbaník**
Studijní program:	**Kybernetika a robotika**
Obor:	**Letecké a kosmické systémy**
Název tématu česky:	**Kompaktní aerometrická sonda**
Název tématu anglicky:	**Compact Aerometrical Probe**

Pokyny pro vypracování:

Cílem projektu je návrh aerometrické sondy umožňující měření rychlosti letu, výšky letu, úhlu náběhu a vybočení. Součástí práce je návrh mechanického uspořádání, vestavění potřebných senzorů a související elektroniky. Celý systém bude tvořen jedním kompaktním zařízením s digitálním výstupem informace pomocí různých digitálních rozhraní (CAN, RS232, ...). V rámci práce bude provedena kalibrace výsledné sondy ve větrném tunelu.

Seznam odborné literatury:

[1] Cary R. Spitzer, Digital Avionics Handbook, 2006, CRC Press, ISBN-10: 0849384419

[2] Vedral, J., Fischer, J.: Elektronické obvody pro měřicí techniku. Vydavatelství ČVUT, Praha 1999, vydání 2., 340 s., ISBN 80-01-02966-2.

[3] Pačes, P. - Popelka, J. - Auersvald, J.: Standalone Trailing Probe for Aerometrical Measurements. In DASC 2012 - 31th Digital Avionics System Conference - Proceedings. Piscataway: IEEE Operations Center, 2012, vol. 1, art. no. 1, p. 1-12. ISSN 2155-7195. ISBN 978-1-4673-1698-9.

Vedoucí diplomové práce:	doc. Ing. Pavel Pačes, Ph.D.
Datum zadání diplomové práce:	10. prosince 2015
Platnost zadání do[1]:	30. září 2017

L. S.

Doc. Ing. Jan Holub, Ph.D.
vedoucí katedry

Prof. Ing. Pavel Ripka, CSc.
děkan

V Praze dne 10. 12. 2015

[1] Platnost zadání je omezena na dobu tří následujících semestrů.

Acknowledgement

I would like to thank my supervisor doc. Ing. Pavel Pačes, Ph.D. for guidance through the work on my diploma. Also I would like to thank Ing. Petr Kočárník for help with physical description of airflow inside the tube, and Ph.D. Ing. Tomáš Čenský, Ph.D. for providing manufacturing of the probe.

I'm grateful to my family and my girlfriend for providing support throughout my studies.

Prohlášení autora práce

Prohlašuji, že jsem předloženou práci vypracoval samostatně a že jsem uvedl veškeré použité informační zdroje v souladu s Metodickým pokynem o dodržování etických principů při přípravě vysokoškolských závěrečných prací.

Author statement for undergraduate thesis:

I declare that the presented work was developed independently and that I have listed all sources of information used within it in accordance with the methodical instructions for observing the ethical principles in the preparation of university theses.

Prague, date..... .....

signature

Anotace

Pro měření rychlosti letu, výšky letu, úhlu náběhu a úhlu vybočení letadla se obvykle používá několik přístrojů. Cílem této práce je navrhnout kompaktní zařízení bez pohyblivých částí, které zkombinuje všechny tyto funkce. Toho je dosaženo vyhodnocováním vzduchového toku kolem těla sondy. Tato práce zahrnuje návrh desky plošných spojů, která řídí sondu a poskytuje výstup naměřených dat. Navržená sonda byla vyrobena a sestavena.

Klíčová slova

aerometrická sonda, pitot-statická sonda, měření rychlosti letu, měření úhlu náběhu, měření úhlu vybočení

Annotation

Conventionally, for measuring airspeed, altitude, angle of attack and angle of sideslip of an aircraft, multiple flight instruments are used. The aim of this thesis is to design a rigid aerometric probe, which combines all of the functions stated above, while being compact. This goal is accomplished by evaluating airflow around the body of the probe. This work includes design of the printed circuit board, which controls the probe, and provides transmission of the acquired data. The designed probe was manufactured and assembled.

Keywords

aerometric probe, pitot-static probe, airspeed measurement, angle of attack measurement, angle of sideslip measurement

Contents

List of Figures xiii

1 Introduction 1

2 Construction of pitot-static tubes 3
2.1 Pitot-static tube . . . 3
2.1.1 Obstruction of pitot-static system . . . 4
2.2 Total pressure measurement . . . 5
2.2.1 Factors influencing total pressure measurement . . . 5
2.3 Static pressure measurement . . . 11
2.3.1 Construction of static pressure tubes . . . 11
2.4 Methods of measuring angle of attack . . . 14
2.4.1 Pivoted vane . . . 15
2.4.2 Null-seeking pressure tube . . . 15
2.4.3 Differential pressure tube . . . 15

3 Proposed mechanical design of the probe 17
3.1 Head of the probe . . . 17
3.2 Static pressure measurement . . . 18
3.3 Draining of the aerometric probe . . . 19
3.4 Discussion . . . 19

4 Proposed electronic design of the probe 23
4.1 Schematic design . . . 23
4.1.1 Pressure sensors . . . 23
4.1.2 Power supply . . . 27
Input capacitors . . . 29
Inductor . . . 29
Output capacitors . . . 29
Boot-strap capacitor . . . 29
Power diode . . . 29
Input protection . . . 30
4.1.3 Heating of the probe and temperature measurement . . . 30
4.1.4 Interface . . . 31
4.1.5 Microcontroller . . . 32
4.1.6 Open drain output . . . 32
4.1.7 D-Sub connector . . . 33
4.2 Printed circuit board design . . . 33
4.2.1 Layout of the switching power supply . . . 34
4.2.2 Microcontroller layout . . . 36
4.2.3 Power distribution layers . . . 36

5 Conclusion 37

Appendices

A Tables and schematics **39**

B CD content **43**

Bibliography **44**

List of Figures

1 A schematic drawing of a pitot-static tube. 3
2 A typical electrically heated pitot-static tube [5, page 5-2]. 4
3 Shapes of total pressure tubes: hemispherical(a), cylindrical(b), conical(c) and ogival(d). 6
4 Total pressure tubes [8]. 7
5 Effect of size of impact opening on impact-pressure error. Total pressure tube with hemispherical tip [7]. 8
6 Drawing of a pressure duct with a drain hole. 9
7 Theoretical pressure distribution along cylindrical bodies [12]. 12
8 Influence of a vertical stem on the static pressure error [12]. 13
9 Static pressure tube with unsymmetrical orifice arrangement [12]. . . . 13
10 Static pressure tube with two orifices at ±30° from bottom [12]. 14
11 Effect of orifice diameter [14]. 14
12 Effect of edge shape of orifices. Static pressure error of each edge shape referenced to square-edge orifice of 0.8 mm diameter [14]. M = 0.4 to 0.8. 14
13 Nose-boom with two pivoted vanes [2]. 15
14 Null-seeking pressure tube [2]. 16
15 Two differential pressure tubes with hemispherical tips, having orifices spaced 60° and 90° apart and their variation of pressure difference in proportion of dynamic pressure ($\Delta p/q$) with AoA (α) [2]. 16

16 Overview of the aerometric probe. 17
17 Head of the probe. 18
18 Placement of static pressure orifices. 19
19 Static pressure chamber with heating element, thermistor hole and static pressure outlet. 20
20 Means of removing water from pressure ducts and from inside the probe. 21

21 A block schematic of the pcb. 24
22 An arrangement of pressure sensors. 24
23 A schematic drawing of a pressure sensor [16]. 27
24 A schematic drawing of a step-down switching power supply. 28
25 A schematic drawing of a heating switch circuit. 31
26 A schematic drawing of a thermistor circuit. 31
27 A schematic drawing of an RS232 transceiver circuit. 32
28 A schematic drawing of CAN circuit. 32
29 A schematic drawing of an open drain circuit. 33
30 Cross section of a four layer pcb made by Pragoboard [26]. 34
31 Top and bottom view of designed pcb. 35
32 Inner power layer (blue) depicted over top side of the pcb. 36

33 A schematic drawing of a microcontroller. 40
34 D-Sub connector. 41

Chapter 1

Introduction

During flight, a pilot depends on the information provided by flight instruments, such as altitude, airspeed or orientation of the aircraft. Although these instruments are developing throughout the history, their basic principle often remains the same. A good example is the pitot-static tube, which considerably changed its design, but its still used for determining airspeed from the difference between measured pressures.

The knowledge of angle of attack and angle of sideslip is another useful information for the pilot. Traditionally, these angles were measured by moving parts, such as pivoted vanes. In some of the available devices, pivoted vanes are still used for this purpose [1]. A method of measuring angle of attack by a differential pressure tube is known for a long time, but it was not widely-used [2].

Authors of [3] had an idea of combining pitot-static tube with a differential pressure tube for measuring airspeed, angle of attack and angle of sideslip. My task is to improve this device and make it suitable for use on an aircraft.

This thesis is structured as follows:

In chapter 2, mechanical design of pitot-static tubes is analysed. Firstly, I introduce the pitot-static tube as a device for measuring airspeed. After that, I describe respective parts of this device, and how they influence performance of this instrument. Also, methods of measuring angle of attack of an aircraft are discussed in this chapter.

In chapter 3, I present the proposed mechanical design of the aerometric probe. The work in this chapter is based on information in chapter 2.

Chapter 4 contains analysis of the designed circuit board, including schematic design and printed circuit board design of the device. Selection of electronic components is discussed here.

Chapter 2

Construction of pitot-static tubes

In the following text, construction of pitot-static tubes will be analysed, with precautions, that have to be taken to prevent malfunctions of the pitot-static system. I will also mention principles of angle of attack (AoA) and angle of sideslip (AoS) measurement.

2.1 Pitot-static tube

A pitot-static tube is a widely-used device in applications, where the local fluid velocity is measured. On aircraft, pitot-static tubes are used as speedometers.

A schematic drawing of a pitot-static tube is shown in figure 1. The pitot-static tube consists of a tube, which is pointed towards the incoming undisturbed flow. The undisturbed flow is described by its static pressure p_s, density ρ and velocity v. On the tip of the tube, the flow stagnates, which causes the local pressure to rise. The total pressure p_t is a sum of this pressure rise and the static pressure of the undisturbed flow p_s. The tube contains two types of openings, which transfer the total pressure and the static pressure into the pressure transducer: a total pressure opening, which runs in parallel with the incoming flow; and static pressure openings, which are positioned perpendicularly to the incoming flow. The pressure transducer measures the difference

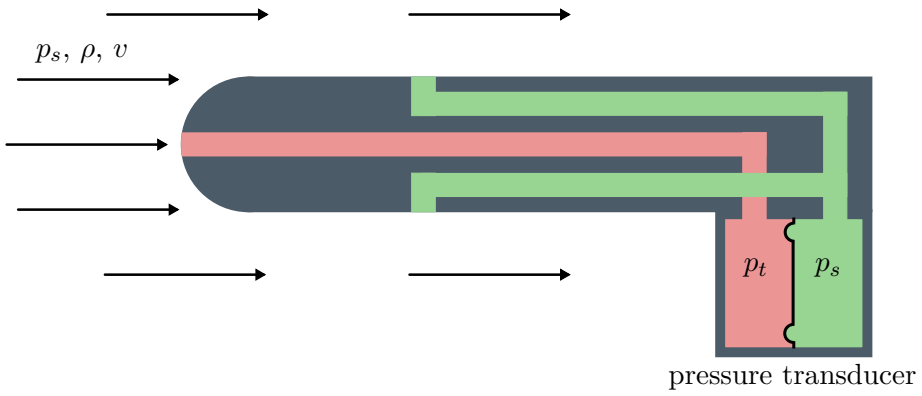

Figure 1 A schematic drawing of a pitot-static tube.

between the static pressure p_s and the total pressure p_t, which we use to determine the velocity v of the incoming flow. Assuming that the flow is incompressible and using

Bernoulli's equation

$$\frac{1}{2}\rho v^2 + p_s = p_t \tag{1}$$

and solving for velocity

$$v = \sqrt{\frac{2(p_t - p_s)}{\rho}},$$

we get the formula for the velocity of the incoming flow [4].

2.1.1 Obstruction of pitot-static system

The knowledge of the airspeed provided by the pitot-static system is crucial for a safe flight. Malfunction of this system could lead to dangerous situations, such as stall or excessive speed. Most of the time, these malfunctions are caused by a blockage of this system. The system can be blocked in many ways, for example moisture, ice, dirt or insects [5]. Pitot-static tubes incorporate several means of preventing these blockages, as shown in figure 2.

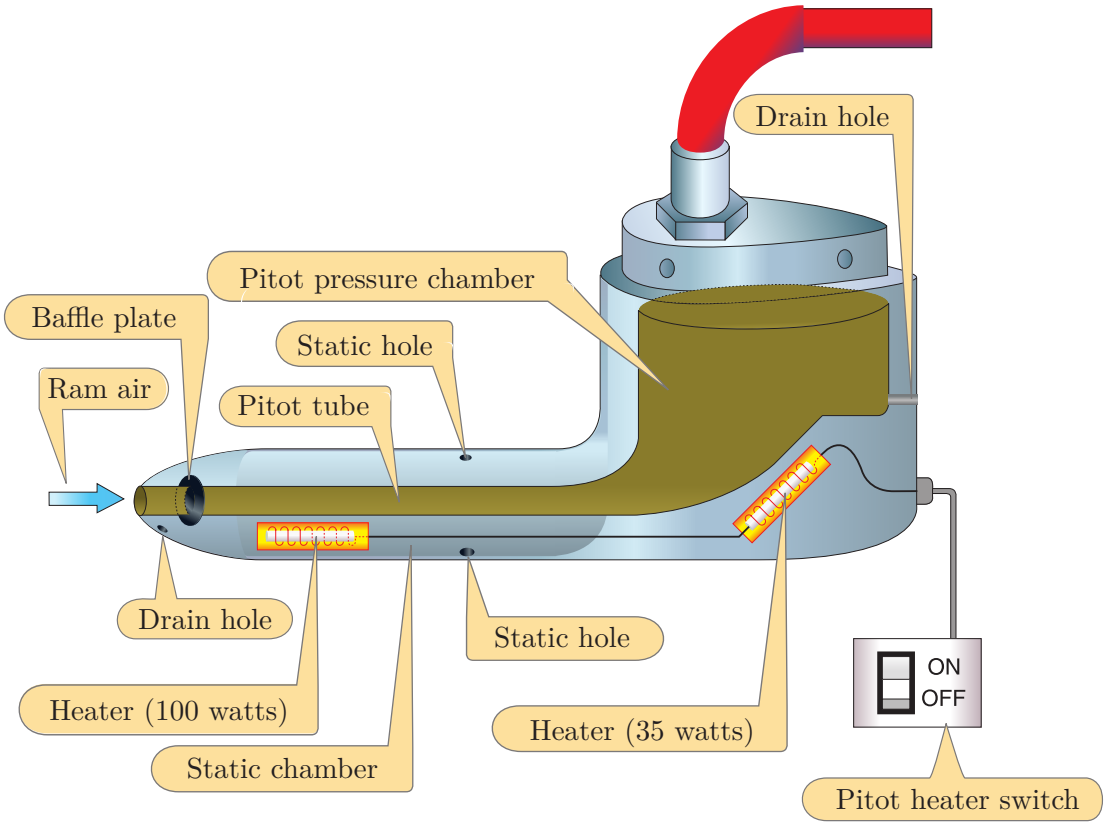

Figure 2 A typical electrically heated pitot-static tube [5, page 5-2].

To deal with moisture, pitot-static tubes have several holes, so the water can drain off. Otherwise, the water could accumulate inside the tube. The first drain hole is usually situated right under the tip of the tube, connected to the inlet of total pressure. It's purpose is to drain water captured in front of a baffle plate. This deflects a large portion of the incoming water, which would normally continue further into the device. The second drain hole is positioned in a more remote parts of the pitot-static tube and drains the water which got through the baffle plate and the water which condensed inside the tube.

To prevent icing, many pitot-static tubes contain a heating element, which rises the temperature of the tube above the freezing point. A pilot can switch on this heating, when he suspects that the conditions for ice forming are met, or when the ice has already formed. The water from the melted ice is then drained through drain holes. Usually, the heating has two or three intensity settings: "off/on", or "off/low/high", and the pilot decides, which one is appropriate.

When the plane is parked for more than a short period of time, pitot-static tubes are covered to prevent contaminants from entering the system. The cover has to be removed during preflight [5, chapter 5].

2.2 Total pressure measurement

To determine the airspeed of the aircraft, the knowledge of both total and static pressure is needed. The principles of measuring these pressures are well-explored. Due to the extent and complexity of this subject, I will try to summarize only the parts, which are relevant for this thesis. Much of the important information, that I left out, can be found in the cited literature, if deeper understanding is desired.

2.2.1 Factors influencing total pressure measurement

In the previous section it was assumed, that the pitot-static tube is pointed towards the incoming flow, so the angle of attack of the tube is 0°. Most of the time during flight, however, the actual angle of attack is non-zero, which influences the total pressure measurement. To limit the measurement error, this fact has to be taken into consideration.

In this section I will discuss several shapes of pitot-static heads with various total pressure openings and their performance in conditions with inclined airstream at subsonic speeds. The performance of the heads will be judged by their range of insensitivity—the range of inclination of the airstream, where the total pressure error is less than 1% of the dynamic pressure. Moreover, effect of drain holes on the total pressure measurement will be discussed. For simplification I will assume that the airstream is not influenced by the presence of other bodies, such as wings or fuselages.

Head shape

A shape of a pitot-static head is one of the things that significantly influence the total pressure measurement. Throughout history, many different types were used. Generally, all pitot-static heads can be divided into two categories: unshielded and shielded.

Unshielded pitot-static heads have simple shapes, such as hemispherical, cylindrical, conical or ogival, as illustrated in figure 3.

The hemispherical tip was used in the early designs—for example, in the well-known Prandtl tube. The accuracy of this head is, however, strongly dependent on inclination. The range of insensitivity of the hemispherical tip is approximately $\pm 5°$ [6]. Despite the low range of insensitivity, pitot-static tubes with hemispherical tips were capable of measuring dynamic pressures with acceptable accuracy up to $\pm 12°$ inclination. This was achieved by designing the pitot-static tube in such a way, that the inclination of the airstream caused a negative total pressure error, which was compensated by a positive static pressure error [7].

Due to the unsatisfactory performance of hemispherical tips in a total-pressure measurement, other shapes were studied. A thorough comparison of cylindrical, conical

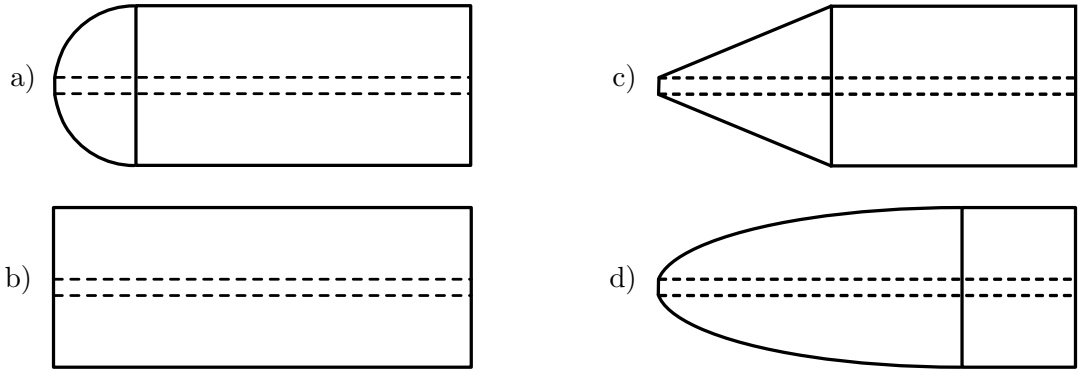

Figure 3 Shapes of total pressure tubes: hemispherical(a), cylindrical(b), conical(c) and ogival(d).

and ogival tips was conducted in [8]. One of the conclusions reached in this study was, that from unshielded tubes the cylindrical tip with suitable total pressure opening has the highest range of insensitivity (±27.5° at a Mach number of 0.26). This tip, labelled as A-9, is shown in figure 4.

The range of insensitivity is symmetrical for heads with square profiles. In applications, where high negative angles of attack are not expected, the tip can be slanted, which shifts the range of insensitivity. For each degree of slant, the positive range of insensitivity can be increased by about 1°, up to 20°. Examples of these tips are in figure 4, labels A-6, E-3 and E-4.

If higher ranges of insensitivity are needed, shielded tubes can be used. Shielded tubes are pitot tubes covered by a cylindrical shield. In [8], the highest range of insensitivity (±63° at a Mach number of 0.26) was achieved with this type of tube. This tube is depicted in figure 4, labelled as A_S-12. Shielded tubes will not be discussed further, because it exceeds the scope of this thesis.

Total pressure opening

An important part, which greatly influences the range of insensitivity of a total pressure head, is the total pressure opening and its size and shape.

Figure 5 shows how impact pressure error of a hemispherical tip depends on size of the total pressure opening. The test was conducted for different angles of yaw Θ (symmetrical tubes have similar behaviour when inclined horizontally and vertically). It can be seen, that for any Θ, the error decreases, as the size of the opening increases. This holds true for cylindrical, conical and ogival tips as well.

The tubes depicted in figure 4 differ in the design of the internal pressure chamber. For example, the tube A-2 has a cylindrical internal chamber, A-5 hemispherical and A-7 conical. Authors of the report [8] stated, that from the cylindrical tubes, the ones having conical internal chambers had the greatest range of insensitivity (±24.5° at a Mach number of 0.26). The tested tubes had internal chambers of the same length, so the differences in angles of insensitivity were caused solely by the shape of the chamber. The performance of the tubes with conical internal chambers can be further increased by lowering the angle of the internal cone, reaching its maximum potential at around 30°.

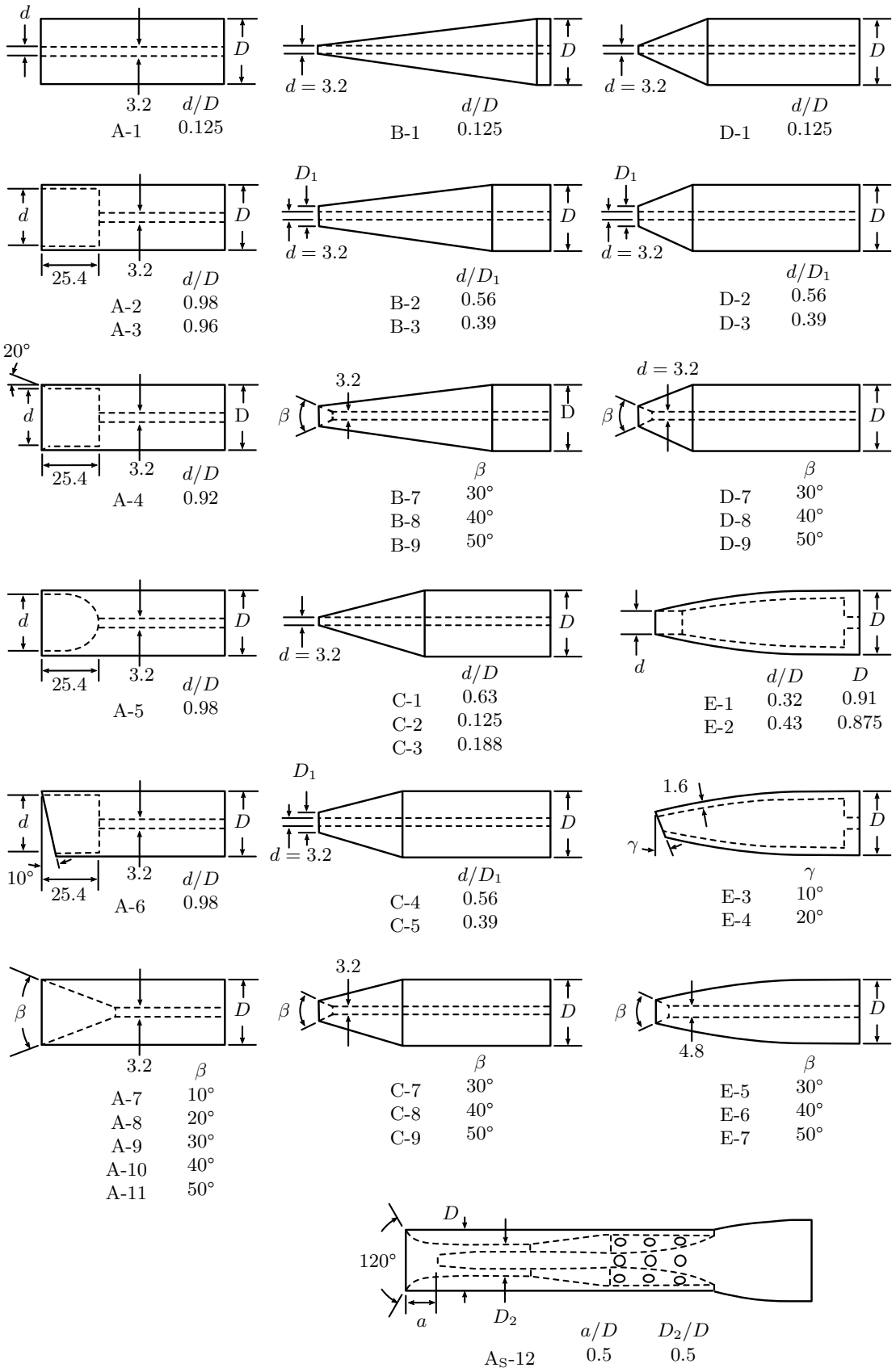

Figure 4 Total pressure tubes [8].

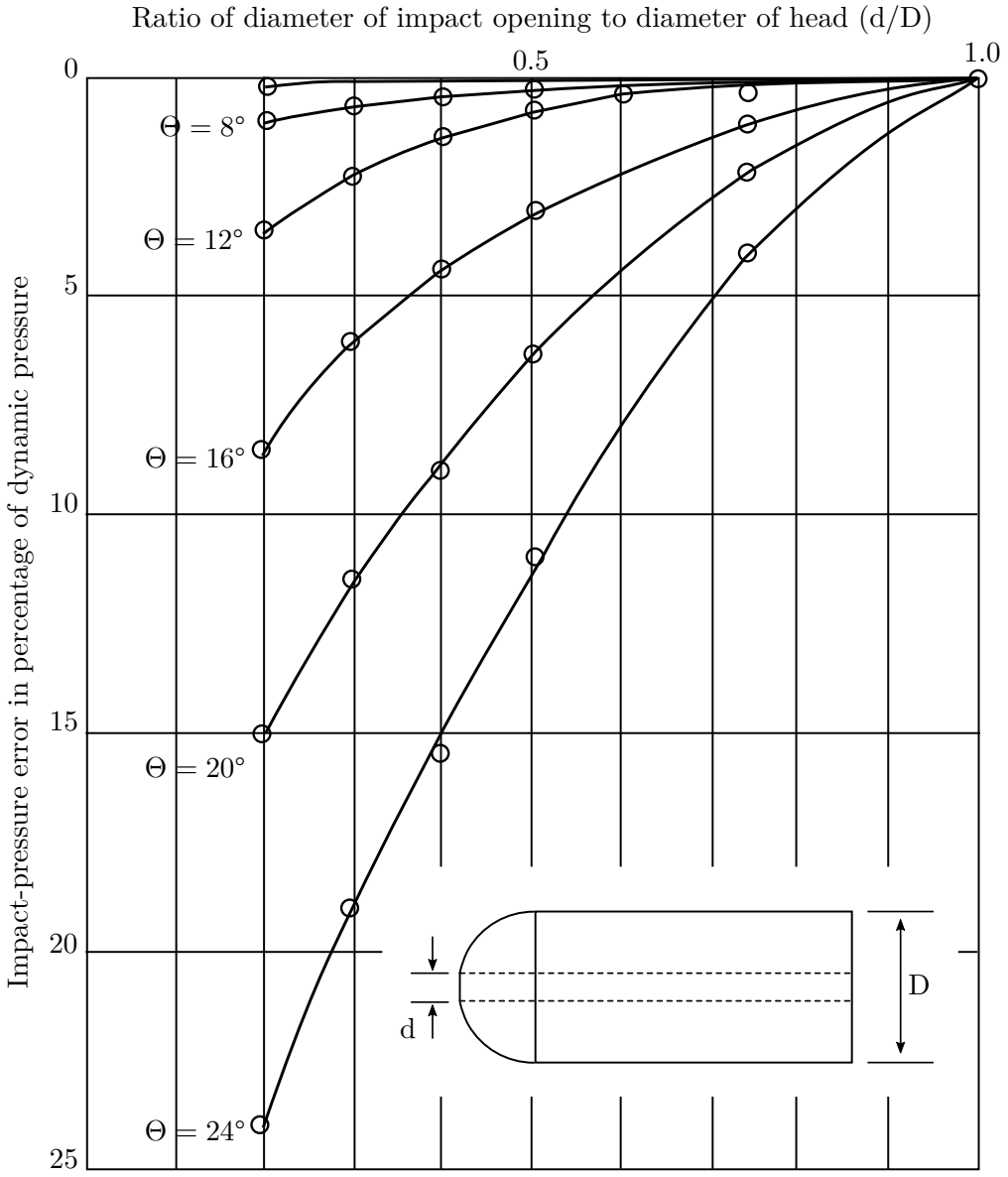

Figure 5 Effect of size of impact opening on impact-pressure error. Total pressure tube with hemispherical tip [7].

Drain holes

Drain holes are an important part of the pitot-static system. If water or other impurities get inside the pressure-conducting tubes, it could cause blockage, which would led to erroneous pressure readings. Because drain holes are basically openings in the pressure system, their presence can affect pressure measurement. Unfortunately, I couldn't find a thorough examination of pitot-static system draining techniques. Authors of [9] and [10] agree, however, that the error introduced by the usage of drain holes in the available devices is small.

In a widely-cited report [11], estimation of the error in a total pressure measurement caused by the usage of drain holes is presented. This report, however, lacks detailed description of the used pitot-static probe. Furthermore, it includes only the effect of drain holes on the measured pressure, not on the final calculated speed. Having troubles finding another source of information in this area, I asked Ing. Petr Kočárník, Ph.D to

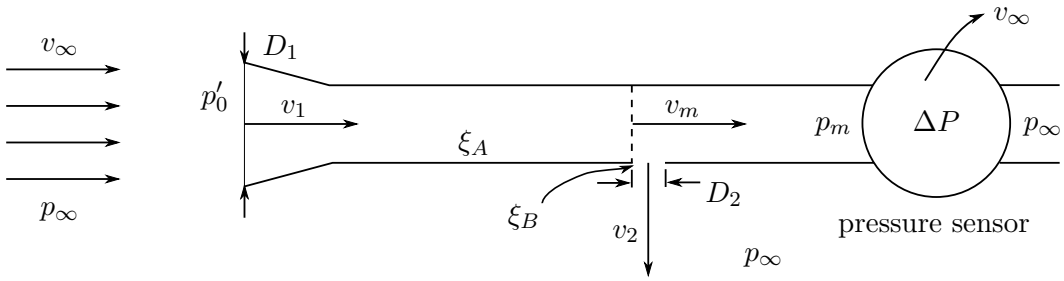

Figure 6 Drawing of a pressure duct with a drain hole.

help me with derivation of the expected error caused by the presence of drain holes in the pressure system.

In figure 6, a pressure duct with a drain hole is depicted. The device is placed into airstream characterized by its speed v_∞ and static pressure p_s. At the orifice with diameter D_1 and area A_1, part of the airstream is slowed down, which increases local pressure p_0'. The pressure p_0' is not a true stagnation pressure p_0, because the airstream enters the pressure duct at a speed v_1—this is caused by the presence of a drain hole in the pressure system. As the airstream continues through the duct, part of its energy dissipates, due to the loss factor ξ_A of the tubing. At the drain hole, the airstream has speed v_m and pressure p_m. The pressure p_m is the measured pressure; there's no air flowing through the pressure sensor and the pressure duct after the drain hole, which would dissipate energy. The air is flowing at speed v_2 from the area with pressure p_m, through the drain hole with diameter D_2, area A_2 and loss factor ξ_2 to area with static pressure p_s.

Summary of the symbols used in the following text:

p_s static pressure of the airstream
v_∞ speed of the airstream
p_0 stagnation pressure of the airstream (total pressure)
D_1 diameter of the pressure inlet
A_1 area of the pressure inlet
p_0' pressure at area A_1
v_1 speed at the pressure inlet
D_2 diameter of the drain hole
A_2 area of the drain hole
v_2 speed through the drain hole
v_m speed right before the drain hole
p_m pressure measured by the pressure sensor
ξ_A loss coefficient of the tubing before the drain hole
ξ_B loss coefficient of the drain hole
ρ density
$v_{\infty m}$ measured airspeed
$v_{\infty true}$ true airspeed

Firstly, we define relative error k_1 of the stagnation pressure p_0:

$$k_1 = \frac{(p_0 - p_s) - (p_m - p_s)}{p_0 - p_s} = \frac{p_0 - p_m}{p_0 - p_s} = \frac{\Delta p_0}{p_0 - p_s}$$

From equation of continuity, we can derive the relation between velocity v_1 at area A_1 and velocity v_2 at area A_2:

$$v_1 A_1 = v_2 A_2 \implies v_1 = v_2 \frac{A_2}{A_1}$$

Bernoulli's equation can be applied to describe flow between airstream and tip of the tube,

$$\frac{v_\infty^2}{2} + \frac{p_s}{\rho} = \frac{v_1^2}{2} + \frac{p_0'}{\rho} = \frac{p_0}{\rho}$$

and to describe flow through the tube:

$$\frac{p_0'}{\rho} + \frac{v_1^2}{2} = \frac{p_0}{\rho} = \frac{p_m}{\rho} + \frac{v_1^2}{2} + \xi_A \frac{v_1^2}{2} \tag{2}$$

$$\frac{p_0'}{\rho} + \frac{v_1^2}{2} = \frac{p_0}{\rho} = \frac{p_s}{\rho} + \frac{v_2^2}{2} + \xi_A \frac{v_1^2}{2} + \xi_B \frac{v_2^2}{2}. \tag{3}$$

Modifying equation 2 and 3 to the following form:

$$\frac{p_0 - p_m}{\rho} = \frac{v_2^2}{2} \left[1 + \xi_A\right] \left(\frac{A_2}{A_1}\right)^2$$

$$\frac{p_0 - p_s}{\rho} = \frac{v_2^2}{2} \left[1 + \xi_B + \xi_A \left(\frac{A_2}{A_1}\right)^2\right]$$

and dividing them between themselves, we get the following formula:

$$\frac{p_0 - p_m}{p_0 - p_s} = k_1 = \frac{1 + \xi_A \left(\frac{A_2}{A_1}\right)^2}{1 + \xi_B + \xi_A \left(\frac{A_2}{A_1}\right)^2}.$$

Assuming, that

$$\xi_A \left(\frac{A_2}{A_1}\right)^2 \ll 1 + \xi_B,$$

we can write

$$k_1 \cong \frac{1 + \xi_A}{1 + \xi_B} \left(\frac{A_2}{A_1}\right)^2.$$

The fraction

$$\frac{1 + \xi_A}{1 + \xi_B} \leq 1,$$

thus

$$k_1 \overset{max}{\cong} \left(\frac{A_2}{A_1}\right)^2 \overset{max}{\cong} 10^{-4}.$$

If

$$\frac{D_2}{D_1} \approx 10^{-1} \implies \frac{A_2}{A_1} \approx 10^{-2} \implies \left(\frac{A_2}{A_1}\right)^2 \approx 10^{-4},$$

then the relative error

$$k_1 \overset{max}{\cong} 10^{-4}.$$

Measured airspeed:

$$v_{\infty m} = \sqrt{\frac{2(p_0 - \Delta p_0 - p_s)}{\rho}} = \sqrt{\frac{2(p_0 - k_1(p_0 - p_s) - p_s)}{\rho}} = \sqrt{\frac{2(p_0 - p_s)}{\rho}} \sqrt{1 - k_1},$$

thus

$$v_{\infty m} = v_{\infty true}\sqrt{1-k_1}.$$

Finally, we can estimate relative error of the measured airspeed:

$$k_2 = \frac{-v_{\infty true}\sqrt{1-k_1} + v_{\infty true}}{v_{\infty true}} = -\sqrt{1-k_1} + 1 \cong -\sqrt{1-10^{-4}} + 1 \cong -5 \cdot 10^{-5}$$

As we can see, if the diameter of a drain hole is 10 times smaller than the diameter of a pressure inlet, we can expect an error of -0.005% in the measured airspeed, which is negligible.

2.3 Static pressure measurement

Many on-board devices, such as altimeter or speedometer, need accurate information about the surrounding static pressure. Throughout history, many methods of acquiring static pressure reading have been developed. These methods are often based on orifices in the aircraft fuselage, or perforated tubes connected to the aircraft. To function properly, these orifices have to be placed perpendicularly to the incoming airstream. This requirement, however, is impossible to fulfil in all flight conditions, so the task of finding the right place for the orifice becomes a task of finding the place, where the static pressure varies the least. This orifice is sometimes placed on a nose-boom, because with increasing distance from the aircraft body, the influence on the static pressure weakens. Another fact which complicates this matter is, that the each aircraft configuration has a unique airflow around its fuselage [12].

In this section, I will describe the method of measuring static pressure using a static pressure tube, which is often combined with a total pressure tube. The device is then called a pitot-static tube.

2.3.1 Construction of static pressure tubes

Similarly to total pressure measurement, accurate static pressure measurement is also dependent on an appropriate construction of the measuring device. Since every object, that is placed into airflow, influences this airflow to some extent, we have to be aware of these influencing factors, and find a suitable place for the static pressure orifices. The problem can be divided into two parts: first, having the tube aligned with the flow; and second, considering that the tube is inclined to the flow. These problems are approached separately. When designing a static pressure tube, these are the main factors that have to be considered:

- shape of the tube tip
- horizontal distance from the tip of the tube to orifice plane
- distance from the vertical stem to orifice plane
- arrangement of the orifices
- orifice diameter and edge shape

Problems caused by inclining the tube to the airflow could be prevented by usage of a swivelling tube. These tubes are, however, considered fragile and efforts are made to design rigid tubes with acceptable characteristics in inclined positions. The performance of a static pressure tube in inclined position depends mostly on arrangement of the orifices [12].

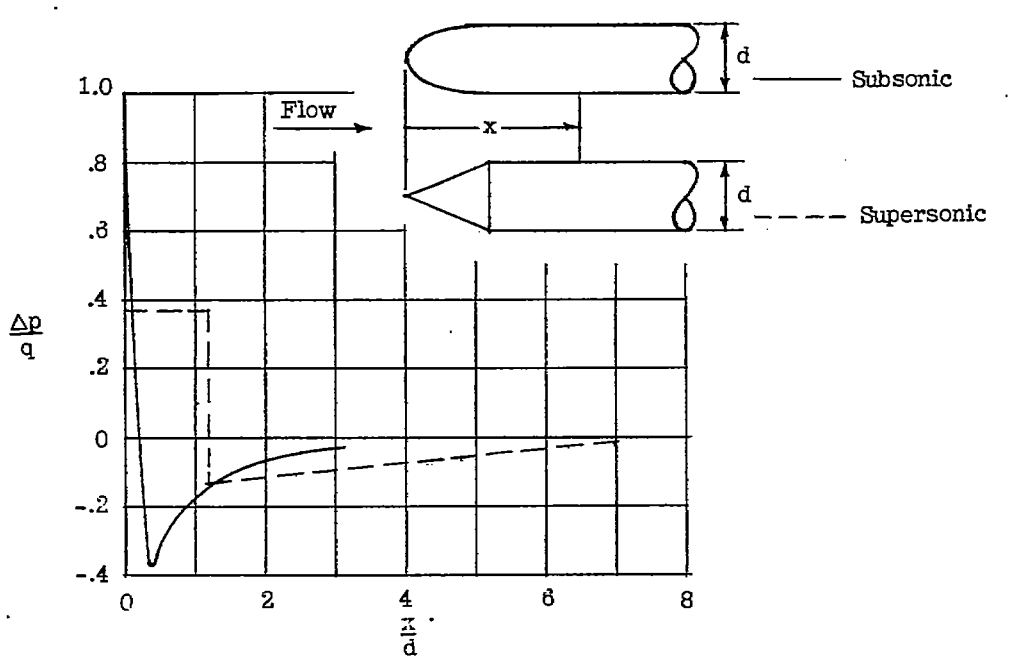

Figure 7 Theoretical pressure distribution along cylindrical bodies [12].

Horizontal distance from the tip of the tube to orifice plane

Static pressure tube placed into airflow creates local pressure disturbances. To prevent static pressure errors, orifices have to be placed in a sufficient distance behind the tip. Although each shape of the tip influences the local pressure distribution differently, tests of hemispherical, ogival and truncated ogival tips at $M = 0.3$ to 0.95 showed, that if the orifices were placed 4 or more tube diameters behind the curvature of the tip, the static pressure errors were almost the same [12]. In figure 7 is shown, how the pressure varies along cylindrical bodies. It can be seen, that at distances greater than 2 tube diameters, the pressure error decreases relatively slowly, and the ideal place for static pressure orifices is somewhere after 3 tube diameters.

Distance from the vertical stem to orifice plane

A presence of other bodies behind the orifice plane, such as vertical stems or collars, creates disturbances, which affect the static pressure measurement. The magnitude of these disturbances depends on thickness of the other body. Figure 8 shows the influence of a vertical stem on the static pressure error. The positive pressure error caused by the vertical stem is sometimes used to compensate for the negative pressure error caused by the tip of the tube [12].

Orifice arrangement

When a cylindrical tube is placed into airflow in inclined position, the pressure difference under the tube is positive, over the tube negative and is zero at locations approximately $\pm 30°$ from bottom of the tube. Therefore, static pressure error can be limited by placing orifices at the top and bottom of the tube, and let the errors subtract, or place orifices at locations of low pressure difference. For reference, if orifices are placed evenly around the tube, the static pressure error reaches -1% of impact pressure at approximately 5° of inclination.

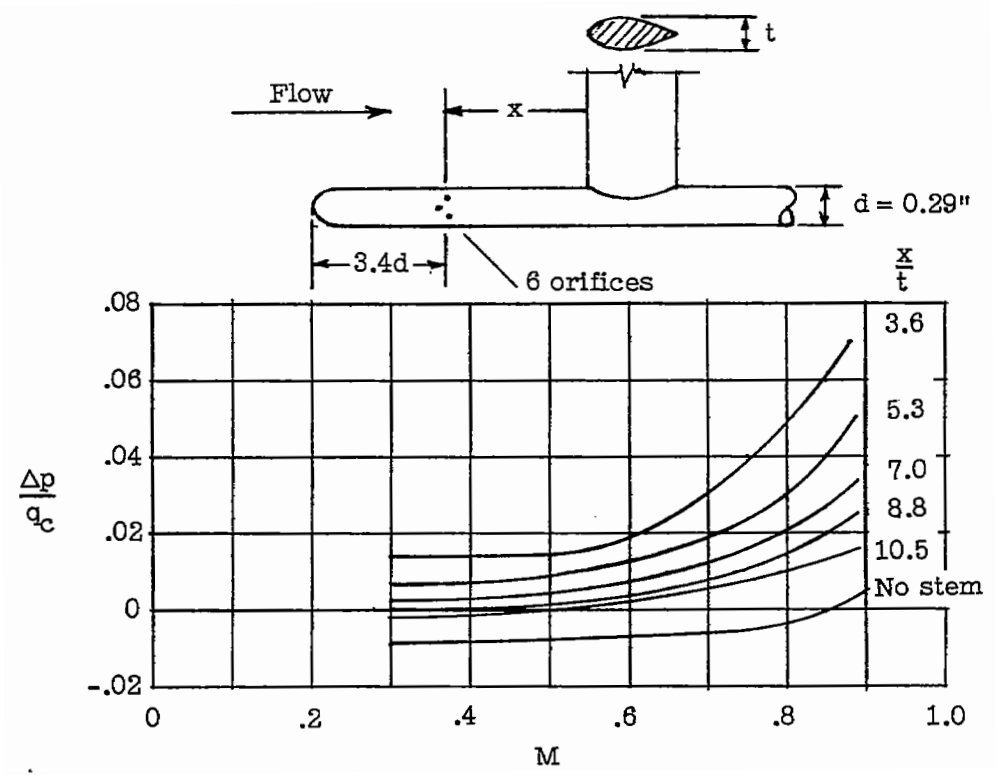

Figure 8 Influence of a vertical stem on the static pressure error [12].

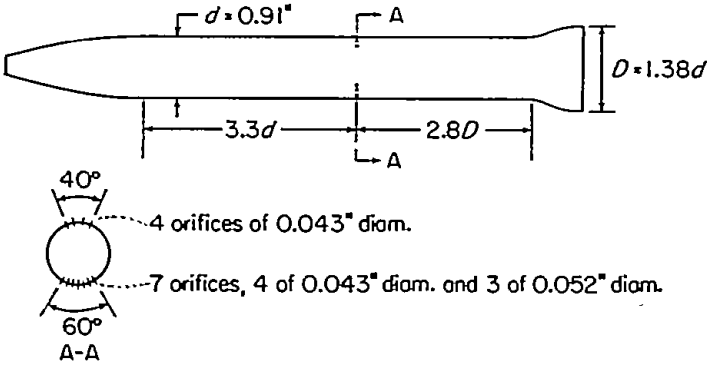

Figure 9 Static pressure tube with unsymmetrical orifice arrangement [12].

Tubes having orifices placed at the top and bottom of the tube have various arrangements. An example of a tube with four orifices at the top and seven at the bottom is shovn in figure 9. With this arrangement, an error of -1% of impact pressure was reached at 40° of inclination at $M = 0.2$.

An example of a tube having two orifices placed at locations of low pressure difference is shown in figure 10. With this arrangement, the static pressure error of -1% of impact pressure was reached at 20° of inclination at $M = 0.3$. Although tubes with this arrangement are more sensitive to angle of attack, the simpler orifice arrangement is easier to manufacture. In another study [13], different probes with orifices spaced 30°, 33°, 36°, 37, 5° and 40° from the bottom of the tube were examined. The conclusion was, that for Mach numbers from 0.4 to 1.0 and inclination of 12°, the tube with orifices spaced 37.5° from the bottom of the tube had the lowest measurement error.

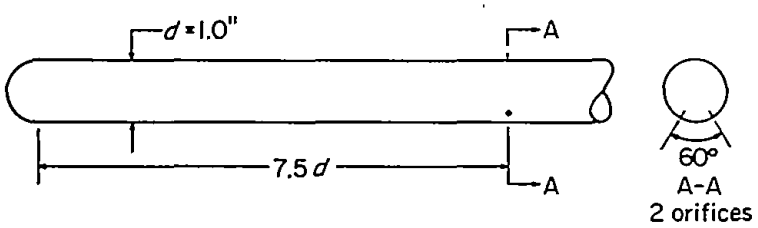

Figure 10 Static pressure tube with two orifices at ±30° from bottom [12].

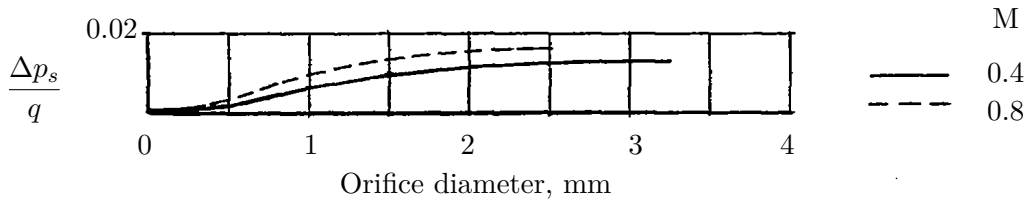

Figure 11 Effect of orifice diameter [14].

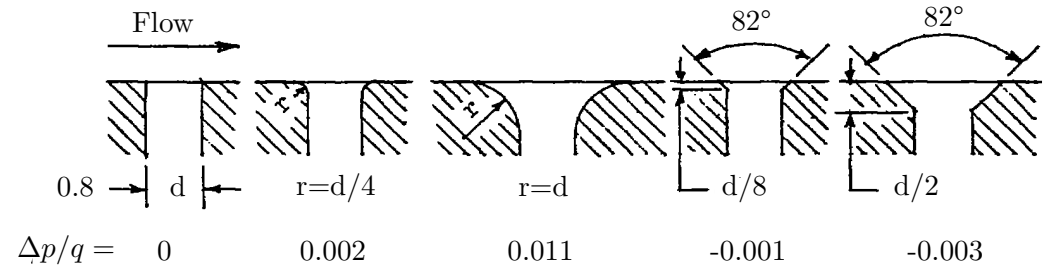

Figure 12 Effect of edge shape of orifices. Static pressure error of each edge shape referenced to square-edge orifice of 0.8 mm diameter [14]. M = 0.4 to 0.8.

Orifice diameter and edge shape

To function properly, orifices have to be drilled accurately and have a smooth surface with sharp edges. In the figure 11 is shown, how the ratio $\Delta p_s/q$ varies with the orifice diameter, where $q = 1/2\,\rho\,v^2$ is a dynamic pressure. It can be seen, that with increasing orifice diameter and Mach number, the static pressure error grows. Although this could lead to a conclusion, that the smallest orifice diameter is the best for the static pressure measurement, the reality is different. The orifices with smaller diameters can be easily blocked, are harder to manufacture and don't leak out water, which condensed inside the tube.

The influence of the edge shape of orifices on static pressure error is shown in figure 12. The errors are referenced to the error of a square-edged orifice of 0.8 mm diameter [14].

2.4 Methods of measuring angle of attack

For a safe flight, it is useful to know the AoA, because many variables such as lift or drag are dependent on it. To obtain this information, three methods are used: the pivoted

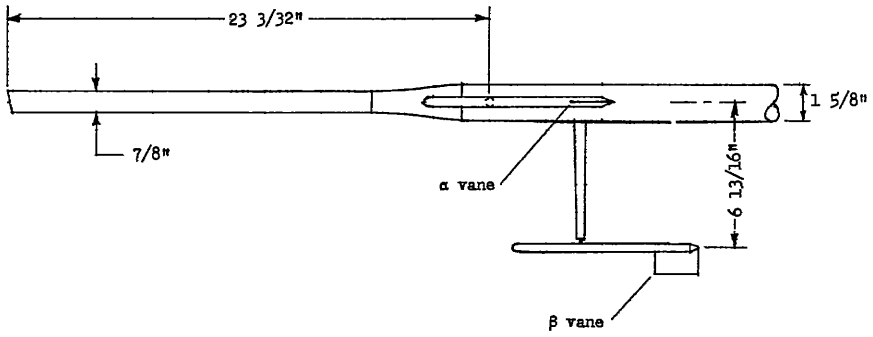

Figure 13 Nose-boom with two pivoted vanes [2].

vane, the null-seeking pressure tube and a differential pressure tube. The examination of the differential pressure tube will be more thorough than the examination of the remaining methods, due to its importance for this thesis. All of the principles described below are usable for AoS measurement as well.

2.4.1 Pivoted vane

A pivoted vane, as the name suggests, is a vane that align itself with the surrounding airflow. This vane can be placed on a nose-boom, under the wing or on the aircraft body. Some of the problems related to usage of pivoted vanes are: oscillations of the vane, fragile construction and that the vane has to be balanced. An example of two pivoted vanes mounted on a nose-boom is shown in figure 13. The α vane is used for measuring AoA and the β vane is used for measuring AoS [2].

2.4.2 Null-seeking pressure tube

A null-seeking pressure tube consists of a rotatable tube with two orifices placed at equal angles from the central plane. The difference between pressures from the two orifices is evaluated by a pressure-sensing device, and the tube is rotated until the pressure difference reaches zero. The AoA can be determined from the rotation angle of the tube. An example of a null-seeking pressure tube is shown in figure 14 [2].

2.4.3 Differential pressure tube

A differential pressure tube is a rigid tube with two orifices at the tip, spaced equally from the central plane. Depending on the AoA, the inclined airflow creates a pressure distribution around the tip of the tube, which causes a measurable pressure difference between the two orifices. The dependence of the pressure difference on inclination is defined by the construction of the tube.

Different shapes of tube tips have different pressure distributions around their body. For a differential pressure tube, it is convenient, that the pressure tube tip creates large pressure difference between orifices when inclined to the airflow. For subsonic speeds, hemispherical tips are used.

The two orifices need to be placed at suitable locations to sense the pressure difference created by the tip. To achieve the largest sensitivity to inclination, orifices have to be placed 90° apart. To some extent, this sensitivity lowers with increasing Mach number. Figure 15 shows two differential pressure tubes with hemispherical tips, having orifices

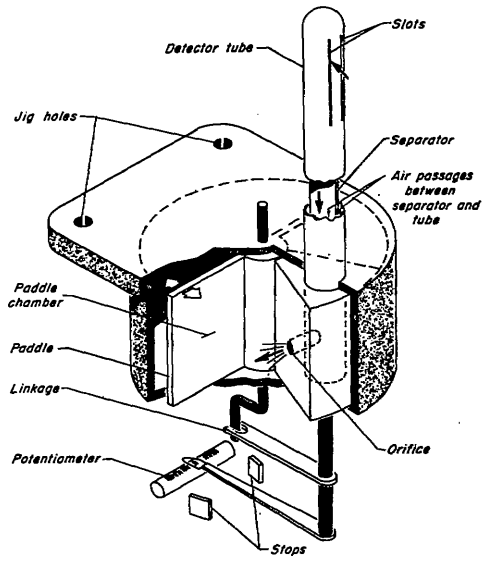

Figure 14 Null-seeking pressure tube [2].

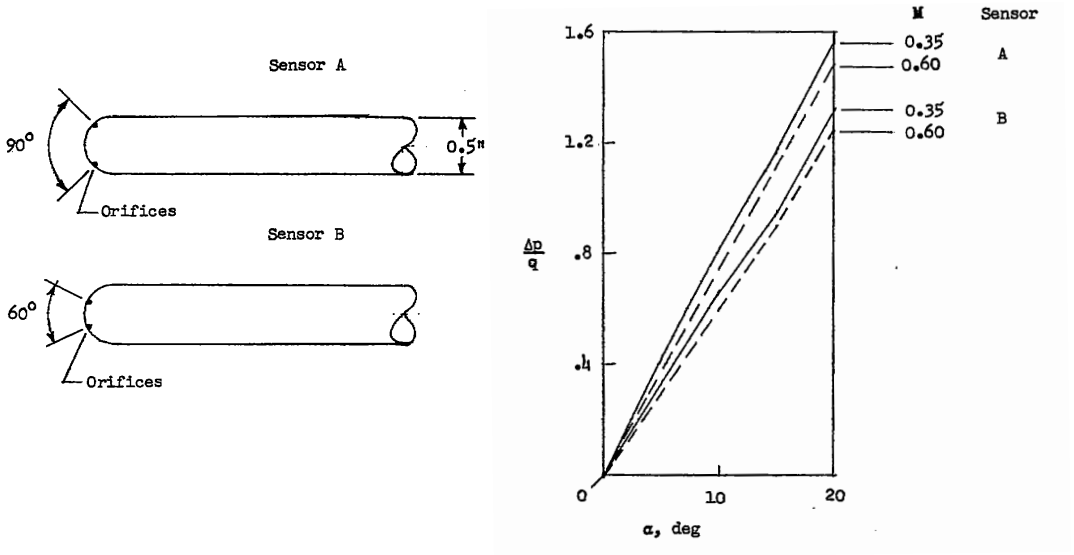

Figure 15 Two differential pressure tubes with hemispherical tips, having orifices spaced 60° and 90° apart and their variation of pressure difference in proportion of dynamic pressure ($\Delta p/q$) with AoA (α) [2].

spaced 60° and 90° apart and their variation of pressure difference in proportion of dynamic pressure ($\Delta p/q$) with AoA (α) [2].

Chapter 3

Proposed mechanical design of the probe

Design of the individual parts is described in the following text. These parts were designed with regards to the information discussed in the chapter 2. For this task, I had learned Autodesk Inventor. Having no previous experience in mechanical engineering, I consulted my work with Ing. Tomáš Čenský, Ph.D., who later provided manufacturing of the elementary parts of the proposed design.

Overview of the aerometric probe is depicted in figure 16. The body of the probe consists of a probe head attached to a tube, which is connected to a vertical stem through an L-joint. To connect the device to an aircraft wing, an attachment pad is used.

The probe has a heated tip and static pressure chamber and incorporates means of removing water from the pressure ducts. The temperature of the probe is measured using two thermistors—one at the tip and one near the static ports.

Pressure ducts run through the L-joint to the vertical stem, where they're connected to pressure sensors.

Most of the probe is made of dural. The vertical stem is made of flat-oval steel tube. To reduce expenses during the design process, we decided to create the L-joint and attachment pad from ABS plastic on a 3D printer.

3.1 Head of the probe

Head of the probe consists of a hemispherical tip. At the front side, facing incoming flow, are two types of openings: a total pressure opening and differential pressure openings. Although there are more suitable shapes for the total pressure head than hemisphere, it was a necessity to make the combination with a differential pressure tube

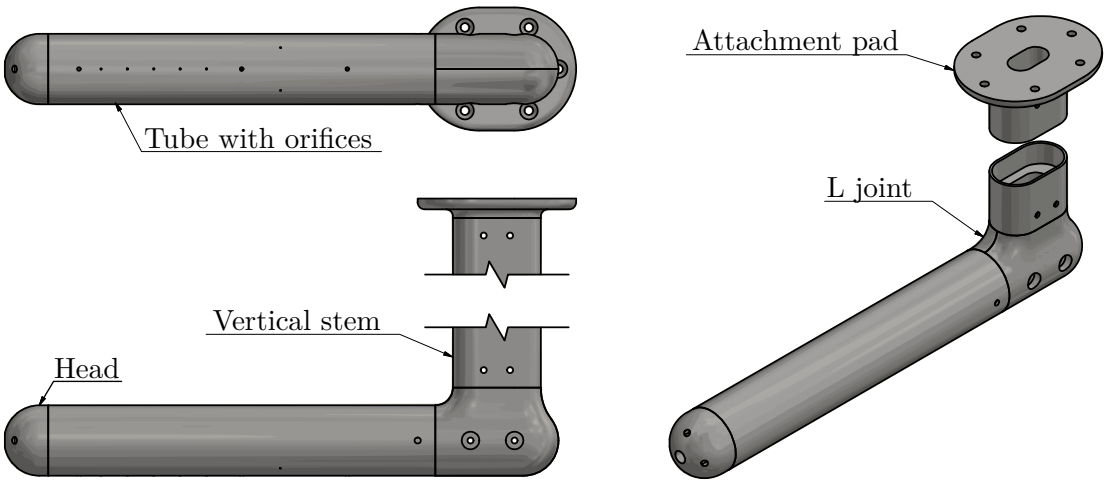

Figure 16 Overview of the aerometric probe.

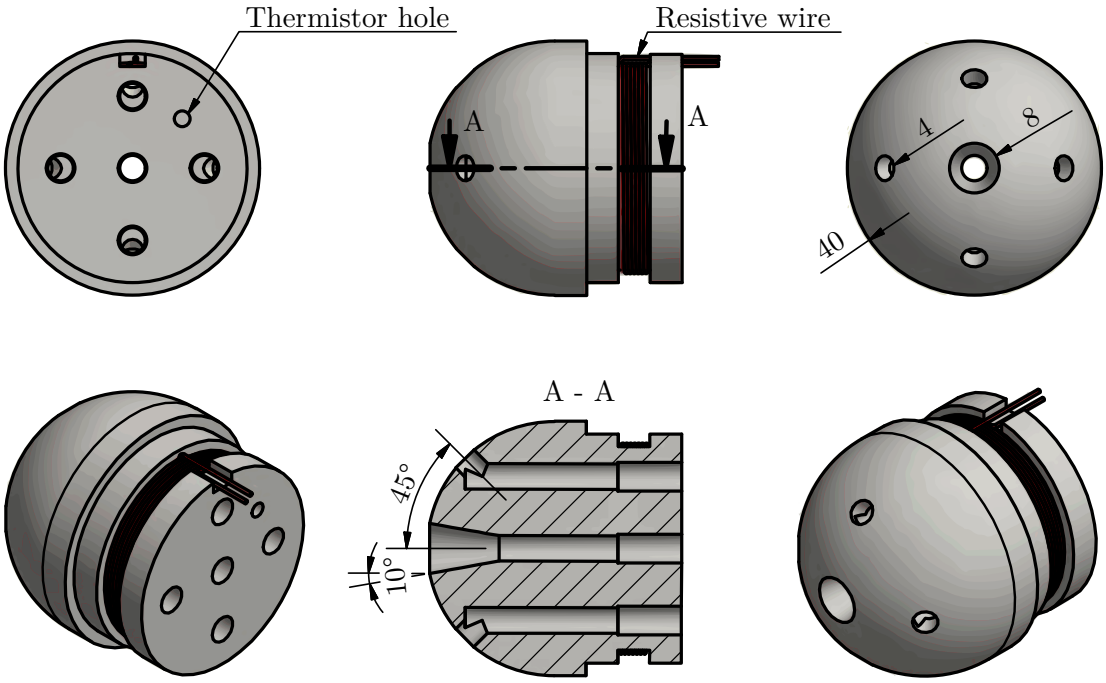

Figure 17 Head of the probe.

possible. According to the discussion in section 2.2.1, increasing the size of the total pressure opening significantly improves the range of insensitivity. Due to the concern that a larger total pressure opening would affect the differential pressure measurement, I chose an opening of a smaller size. The distance between the total pressure port and differential pressure ports was chosen arbitrary, due to the lack of research in this area. The total pressure opening has a 20° internal cone to increase the range of insensitivity, as recommended in section 2.2.1.

The opposing differential pressure openings are spaced 90° apart to achieve the greatest sensitivity to inclination, as described in section 2.4.3.

The head has a groove around its perimeter. In this groove is a coil of resistive constantan wire, connected to a voltage source, functioning as a heating element for this part of the probe. The wire is placed inside PTFE tube, which insulates it electrically from the head, and can withstand high temperatures.

On the back side of the head are pressure outputs from the openings and a thermistor hole. The thermistor is used for temperature measurement. The head of the probe is pictured in figure 17.

3.2 Static pressure measurement

The arrangement of the static pressure ports is based on information discussed in section 2.3.

Static pressure is measured by two orifices with 0.8 mm diameter. The orifices are spaced 37.5° from the bottom of the tube, as depicted in figure 18. The distance from the tip to the orifice plane is 160 mm, which is four times the tube diameter. The distance from the vertical stem to orifice plane is 100 mm, which is more than three times the stem diameter. Ideally, these distances, especially the one from the vertical stem, would be greater, but they should be sufficient to provide satisfactory results while making the aerometric probe compact.

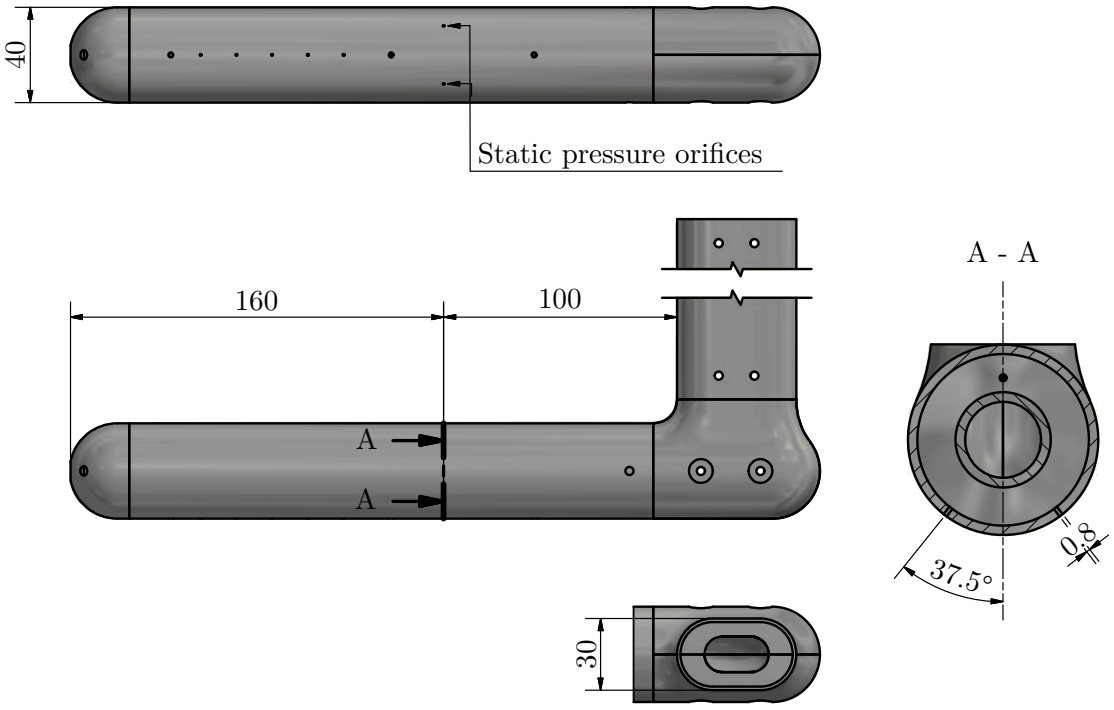

Figure 18 Placement of static pressure orifices.

Inside the tube, besides other things, is a static pressure chamber. The chamber is heated in the same way as the probe head and contains a thermistor for temperature measurement. The static pressure chamber is depicted in figure 19.

3.3 Draining of the aerometric probe

The total pressure port and differential pressure ports are very susceptible to blocking by water or other impurities. To prevent blocking, pressure ducts from pressure ports have greater diameter and are connected to a water trap. The purpose of the water trap is to stop water and other impurities from getting further into the pressure system, which contains thinner pressure ducts and pressure sensors. The tube also contains 3 vents to drain out water which could condense inside the tube.

3.4 Discussion

While I was working on a mechanical design of the probe, I found it difficult to find any recent studies concerned about this topic. Even though I had to research older studies, I believe, that their conclusions are still valid. The biggest problem was to find information about draining of these instruments. This was also the hardest task to solve. While usual pitot-static probes have to incorporate single heated chamber for capturing water, this design requires five—one for each pressure inlet, except static pressure. Because the previous design was neither drained nor heated, I had to come up with a new solution. Before we settled with the water trap described in chapter 3, I had proposed several solutions, which were discarded, due to some concerns—mostly about maintenance and manufacturing.

The best way to provide heating for the probe would be to use an existing solution. Firstly, I tried to find a replacement part for devices that are already on the market.

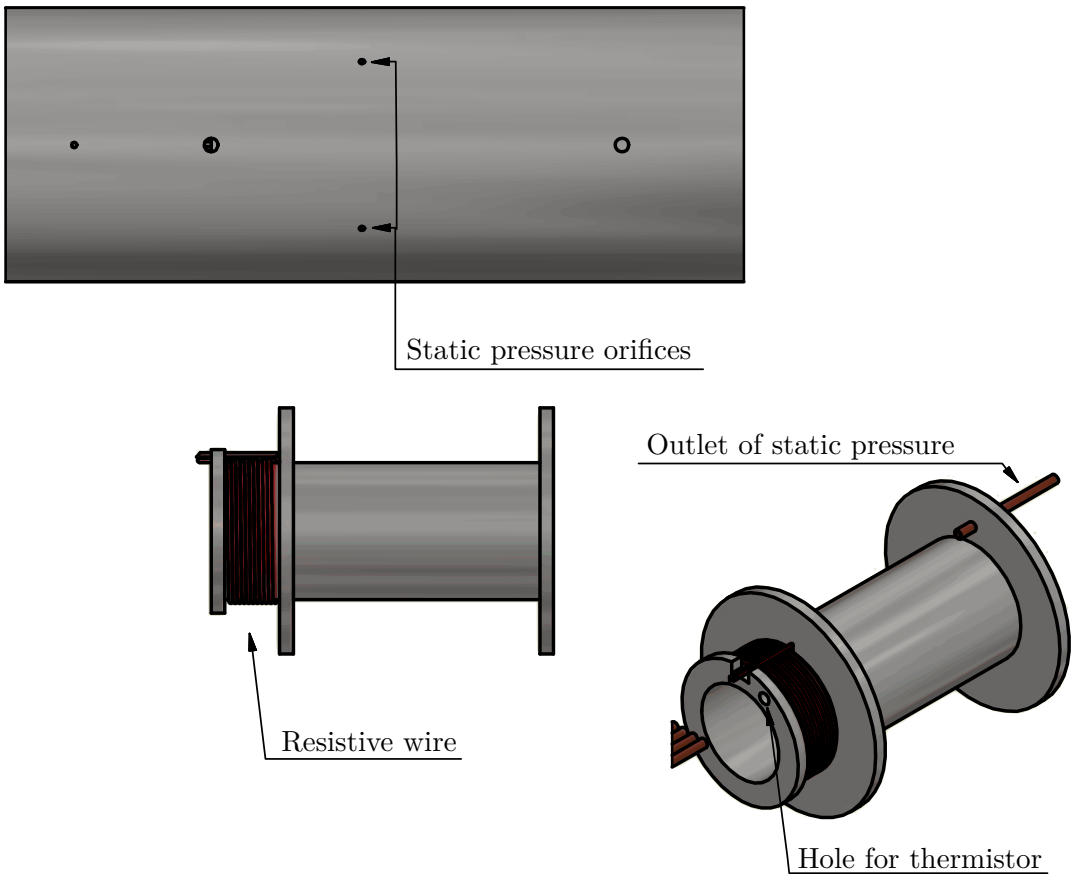

Figure 19 Static pressure chamber with heating element, thermistor hole and static pressure outlet.

I was unsuccessful, so I looked for cartridge heaters made for another purpose. They were either made for different voltage, or had too low/high wattage. In the end, I tried to find an insulated heating wire with desired resistivity. I couldn't find any, so I decided to create my own, made from constantan wire and electrically insulate it.

Heating of the probe, as proposed in this chapter, was assembled and tested. First tests has shown, that it needs improvement. When the input power to the heating coil exceeded approximately 15 W, the temperature of the resistive wire started damaging its PTFE insulation, probably due to the poor heat conduction away from the wire. Because asbestos, which was traditionally used for this purpose, is hard to find nowadays, I have to find another solution to this problem. The next test will include heating wire insulated by a thin kapton tape, which should provide better heat conduction and greater contact area with the surface of the probe. Despite the poor heat conduction and lowered input power, the probe was heating quickly. Because of this, I decided to lower the input power to the coil situated on the head of the probe, and to the one at the static pressure chamber to 75 W and 50 W respectively.

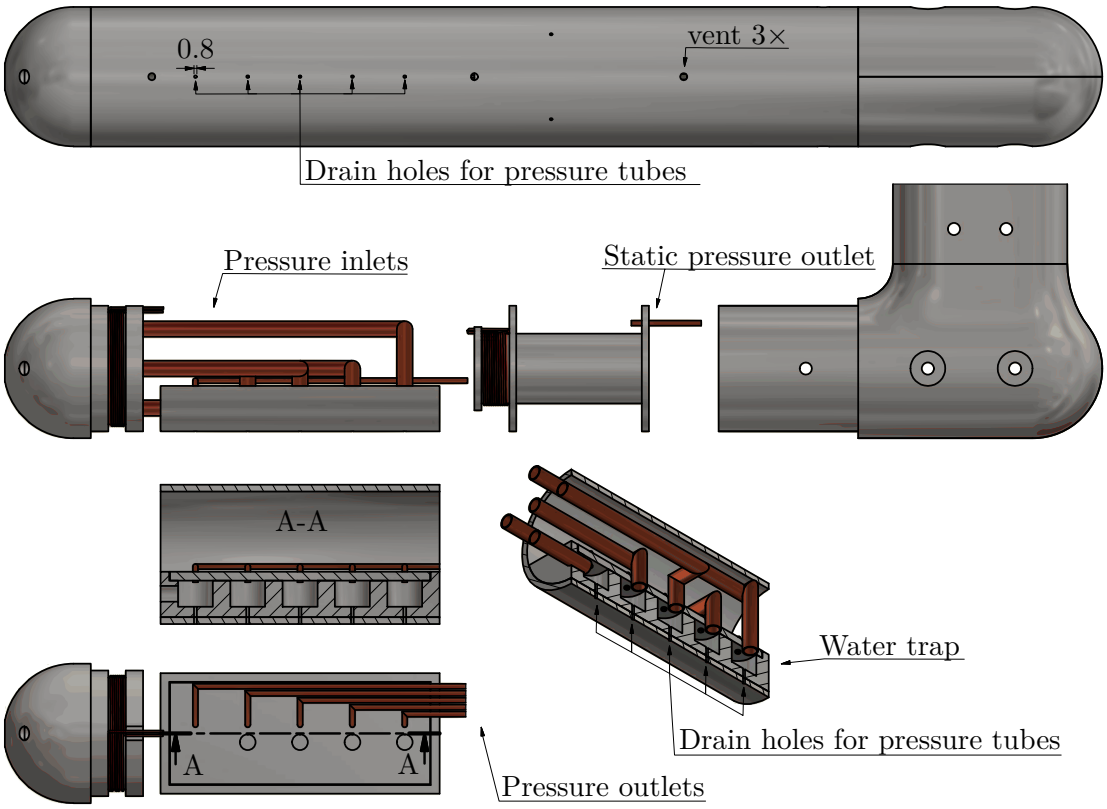

Figure 20 Means of removing water from pressure ducts and from inside the probe.

Chapter 4

Proposed electronic design of the probe

In this chapter, electronic design of the probe will be discussed, including problems, which had to be overcame.

One of the requirements for this work was, that the printed circuit board (pcb) has to be placed inside of the probe. The only not occupied cavity is inside the vertical stem depicted in figure 16, which has a 30×50 mm flat oval cross-section, with 1.5 mm wall thickness. The dimensions of the flat oval cross-section cannot be increased, because it would significantly affect proportions of the rest of the probe. The only way to increase the size of the cavity is to prolong the vertical stem, which is beneficial for the pressure measurement, but causes unfavourable length to width ratio of the pcb. Elongated circuit boards complicate part placement, worsen electromagnetic compatibility (EMC) and are susceptible to mechanical stress, which damages the surface-mounted parts. The goal is based on the facts stated above: create a pcb, which could fit inside the vertical stem, with the smallest length to width ratio, adequately resistant to harsh conditions. During the electronic design, I had put emphasis on the selection of suitable electronic parts for this application.

Firstly, I will discuss the schematic design of the probe. Secondly, the pcb design will be discussed.

4.1 Schematic design

The schematic of the pcb can be divided into several parts, as depicted in figure 21. The device is powered by a 5 V power supply, which should provide stable voltage for the remaining parts. The device is controlled by a microcontroller, which has multiple inputs with analog to digital converters (ADC). These inputs are reading analog values from the pressure sensors and thermistors. If the temperature of the probe falls below a certain value, the microcontroller uses the heating switch to drive a high current through heating wires. The device also contains CAN, RS232 and open drain outputs for communication and signalling.

In the following text, I will describe the individual parts of the schematic.

4.1.1 Pressure sensors

Pressure sensors are a crucial part of the pressure system. They have to measure with great accuracy, which is complicated by their usage in extreme conditions. For this application, two types of pressure sensors will be used: absolute, which measures the pressure relatively to perfect vacuum; and differential, which measures the difference between two pressures. The absolute pressure sensor will be connected to the static pressure outlet, measuring static pressure. The differential pressure sensors will have two functions: measuring differential pressure of the opposing differential pressure ports,

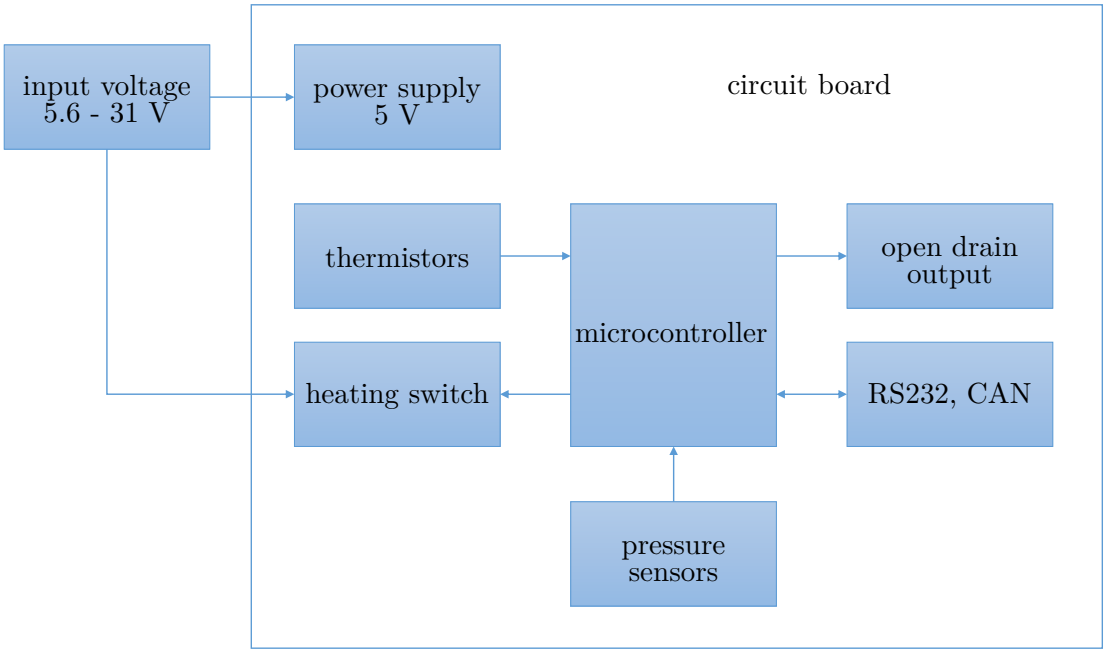

Figure 21 A block schematic of the pcb.

and measuring dynamic pressure. The dynamic pressure will be determined by measuring the pressure difference between the total and static pressure outlets. The outlets are depicted in figure 20 and the arrangement of the pressure sensors is illustrated in figure 22.

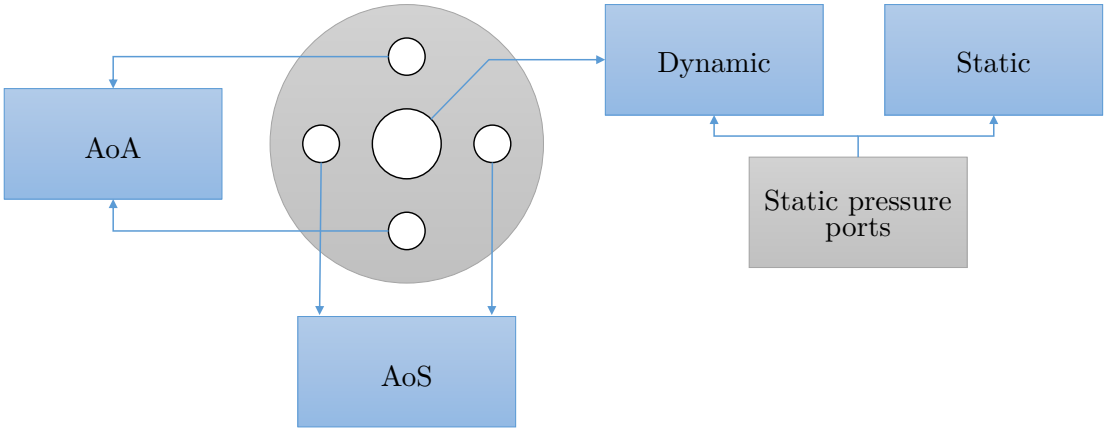

Figure 22 An arrangement of pressure sensors.

Prior to selecting suitable pressure sensors, limit values of atmospheric pressures (both static p_s and dynamic p_d) and temperature t have to be determined. To find the values of p_s and t, I will use the International standard atmosphere (ISA) model. The ISA is a model of the atmosphere developed by the International organization for standardization (ISO). The ISA was recommended by the ISO as a standard for international adoption. Other standard atmospheres, such as the International civil aviation Organization (ICAO) standard and the U.S. standard are identical to the ISA up to 32 km and 50 km respectively.

Temperature

Since our probe will be used in altitudes lower than 11 km, we can calculate the values of t from the following equation [15]:

$$t = T_0 + L\,h, \tag{4}$$

where T_0 is a standard temperature at sea level (=288.15 K), L is a standard temperature gradient ($=-6.5\,\mathrm{K\,km^{-1}}$) and h is a geopotential altitude from sea level.

Static pressure

Below 11 km, the p_s is modelled by the following formula [15]:

$$p_s = P_0 \left[\frac{T_0}{t}\right]^{\frac{g_0\,M_0}{R\,L}}, \tag{5}$$

where P_0 is a standard sea level atmospheric pressure (=101 325 Pa), g_0 is a gravitational acceleration at sea level ($=9.806\,65\,\mathrm{m\,s^{-2}}$), M_0 is a mean molecular weight at sea level ($=28.9644\,\mathrm{kg\,kmol^{-1}}$), R is the universal gas constant ($=8.314\,32\,\mathrm{N\,m\,mol^{-1}\,K^{-1}}$) and t is calculated from equation 4.

Knowing p_s and t, we can also determine the density ρ:

$$\rho = \frac{p_s\,M_0}{R\,t}. \tag{6}$$

Dynamic pressure

To find the limit values of p_d, we'll assume that the flow around the probe is incompressible, and use following equation [4]:

$$p_d = \frac{1}{2}\,\rho\,v^2, \tag{7}$$

where v is a velocity of the incoming flow and ρ is calculated from equation 6. As we can see, if $v = 0$, then $p_d = 0$.

Limit values of $\mathbf{p_s}$ and $\mathbf{p_d}$

Table 1 contains the values of t, p_s and p_d calculated from equations 4, 5 and 7, in the minimal and maximal altitude, in which the tube will be operational. These values, however, are determined from an atmospheric model, and can differ from real conditions.

h (m)	t (°C)	p_s (kPa)	p_d (kPa) for $v = \pm 500\,\mathrm{km\,h^{-1}}$
0	15	101.325	11.815
10000	-50	26.436	3.981

Table 1 Calculated values of t, p_s and p_d

Differential pressure

To decide the pressure range of angle of attack (AoA) and angle of sideslip (AoS) sensors, we have to estimate the maximum pressure difference Δp_{max} between the corresponding ports. According to figure 15, the ratio $\Delta p/p_d$ of a probe with a hemispherical nose shape and pressure ports spaced 90° apart is approximately

$$\frac{\Delta p}{p_d} \approx 1.5,$$

for a 20° AoA(AoS). From this ratio and the maximum value of p_d from Table 1, we can estimate, that $\Delta p_{max} = \pm 18\,\text{kPa}$.

Summary

From the results obtained above, I estimated following pressure ranges:

pressure type	pressure range (kPa)
static	26.436–101.325
dynamic	0–11.815
differential	±18

Table 2 Estimated pressure ranges.

Selected pressure sensors

Pressure sensors were selected according to the following parameters: pressure range, accuracy, compensated temperature, size and price. The selected product series has the best compensated temperature range from the considered options, which is important, since the pcb will be exposed to low temperatures. Absolute pressure sensor Honeywell SSCDRNN015PAAA5 was selected for the static pressure measurement. Although the calculated pressure range for the differential pressure is ±18 kPa, differential pressure sensor with range ±10 kPa Honeywell SSCDRRN100MDAA5 was selected, due to the fact, that airplanes don't fly at high AoA at high speeds. This sensor will be used for measuring dynamic pressure as well. Overview of the selected sensors is in the table 3.

model	range	accuracy	compensated temp.
Honeywell SSCDRNN015PAAA5	0–103 kPa	±2% FSS	-20–85 °C
Honeywell SSCDRRN100MDAA5	±10 kPa	±2% FSS	-20–85 °C

Table 3 An overview of selected pressure sensors.

Schematic drawing

A circuit for the selected pressure sensor is shown in figure 23 [16]. The supply voltage is decoupled by 10 µF and 10 nF capacitor. The output voltage is filtered with a low pass RC filter with cutoff frequency of 650 Hz. The RC filter will not eliminate the need of software averaging of the measured value, but it will lower the frequencies transferred on a pcb, which improves EMC. The circuit also contains 10 nF capacitor, which has to

be connected close to the ADC input pin. The capacitor serves two purposes: the first is, removing noise from the input signal [17]; the second is, providing an immediate source of energy for the internal capacitor of the ADC during conversion. Omitting this capacitor could lead to worsened accuracy of the ADC and increased interference. The capacitance of the external filter capacitor should be

$$C_f \geq 1024\,(C_{INS} - C_{INN}),$$

where C_{INN} is a total input capacitance in a non-sampling phase, and C_{INS} is a total input capacitance in a sampling phase. Fulfilling this requirement, the maximum sampling error of the input voltage should be equal or lower than 1 least significant bit (LSB) of the ADC. In our case, $C_{INN} = 10\,\text{pF}$ and $C_{INS} = 16\,\text{pF}$, so $C_f \geq 6.144\,\text{nF}$ [18]. For this application, I chose 10 nF capacitors in 0603 packages, made from NP0/C0G dielectric. The resistor R23 will not be assembled and provides surface for measuring probe.

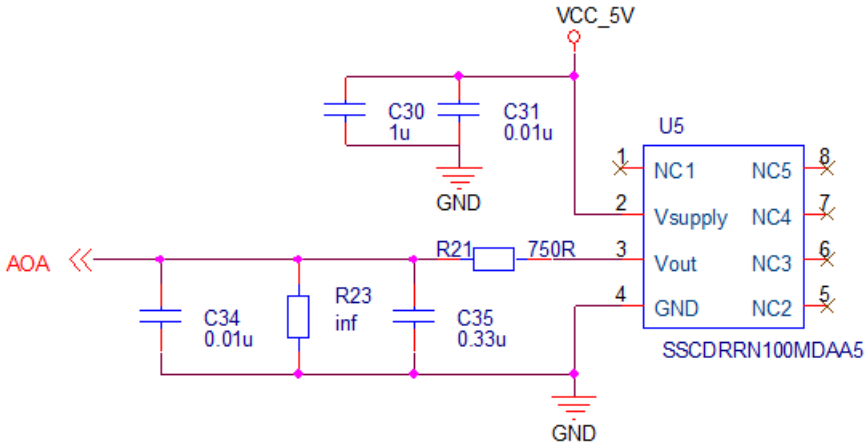

Figure 23 A schematic drawing of a pressure sensor [16].

4.1.2 Power supply

The power supply shown in figure 24 is based on a step-down switching regulator LM22676MRE-5.0 from Texas instruments. The main parameters of this regulator are [19]:

- input voltage range: 4.5 V to 42 V
- output voltage: 5 V
- switching frequency: 500 kHz
- maximum output current: 3 A
- operating junction temperature: −40 °C to 125 °C

The 3 A maximum output current might be excessive for this application. This regulator was chosen, because it has wide input voltage range, high output voltage accuracy, can be used in wide temperature ranges and doesn't need many external components. The documentation [19] contains instructions for selecting external components of the regulator. In the following text, I will follow these instructions to design a suitable power supply for this application.

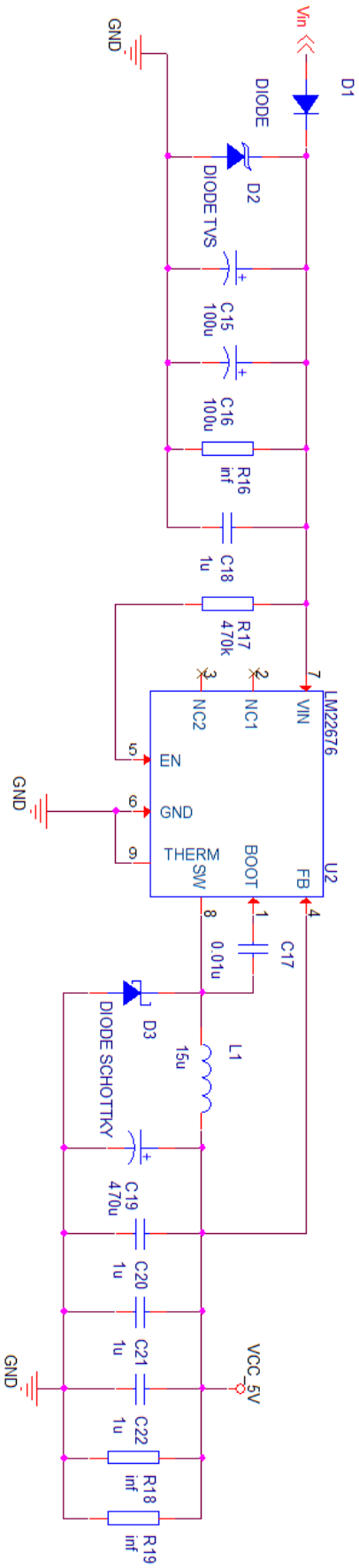

Figure 24 A schematic drawing of a step-down switching power supply.

Input capacitors

The input of the regulator contains two types of capacitors: smaller ceramic capacitor, situated very closely to the regulator, to filter high frequency switching noise; and larger electrolytic capacitors, to filter low frequencies. According to [19], the capacity of the small ceramic capacitor should be between 0.47 µF to 1 µF. In this design, I chose a 1 µF capacitor made from X7R dielectric in a 0805 package. This capacitor is labelled as C18 in figure 24. To filter lower frequencies, two 100 µF electrolytic capacitors are used. Since electrolytic capacitors are known to be prone to malfunctions in modern devices, I chose Vishay capacitors certified for automotive, with wide temperature range [20]. According to [21], electrolytic capacitors from Vishay are usable at low pressures, which are present at high altitudes.

Inductor

According to regulator manual [19], the output current peak-to-peak ripple should be around 30% of the nominal output current. Then, the inductance L of the inductor is calculated as

$$L = \frac{(V_{in} - V_{out})\, V_{out}}{0.3\, I_{out}\, F_{sw}\, V_{in}},$$

where V_{in} is input voltage, V_{out} is output voltage, I_{out} is output current and F_{sw} is switching frequency. For $V_{in} = 28\,\mathrm{V}$, $V_{out} = 5\,\mathrm{V}$, $I_{out} = 1\,\mathrm{A}$ and $F_{sw} = 500\,\mathrm{kHz}$, the inductance of the inductor $L = 27\,\mu\mathrm{H}$. Inductors with this value of L, rated for current of 3 A, were too massive. I had to lower the L, until I found an inductor in a package, that wouldn't increase size of the pcb over permissible limit. Finally, I selected an inductor with $L = 15\,\mu\mathrm{H}$.

Output capacitors

Output capacitors are used for filtering voltage ripple, and for providing energy during transients. Ideally, parallel combination of a larger capacitor (electrolytic or tantalum) with smaller ceramic capacitors is utilized. To filter the output voltage, I chose one 470 µF electrolytic capacitor (C19), from the same series as the input electrolytic capacitors, with three ceramic 1 µF capacitors (C20, C21, C22). With this configuration, the output voltage ripple should be approximately

$$V_{ro} \approx \frac{(V_{in} - V_{out})\, V_{out}}{8\, V_{in}} \cdot \frac{1}{F_{sw}^2\, L\, C_{out}} \approx 0.3\,\mathrm{mV},$$

for $V_{in} = 28\,\mathrm{V}$, $V_{out} = 5\,\mathrm{V}$, $L = 15\,\mu\mathrm{H}$ and $C = 470\,\mu\mathrm{F}$ [19].

Resistors R18 and R19 are not assembled, and provide pads, where additional filter capacitors can be placed.

Boot-strap capacitor

According to [19], a good quality 10 nF capacitor has to be connected between BOOT pin and SW pin. I chose a 10 nF capacitor, made from NP0/C0G dielectric, in a 0603 package.

Power diode

For this application, Schottky diode designed for 3 A maximum forward current and 60 V reverse voltage was selected, to comply with guidelines described in [19].

Input protection

Input of the power supply contains two types of protection: a rectifier diode, which provides protection against reverse polarity of the input voltage; and transient voltage suppressor (TVS) diode, which protects the device against overvoltage.

Maximal forward current of the rectifier diode is 3 A. The rectifier diode causes a voltage drop across its terminals—maximally 1.1 V—which increases the minimal input voltage from 4.5 V to 5.6 V, to provide minimal input voltage for the regulator.

As a protection against overvoltage, I chose a TVS diode Vishay SMCJ28A with stand-off voltage of 28 V. During normal operation, when the input voltage is around 28 V, the TVS diode is practically in a non-conducting state. If the input voltage increases over this value, the TVS diode goes into avalanche breakdown, limiting voltage across its terminals. The breakdown voltage of the selected TVS diode is 31.1 V to 34.4 V [22][23].

4.1.3 Heating of the probe and temperature measurement

To prevent icing of the probe, the device contains two heating coils: one is attached to the head of the probe, and the second is at the static pressure chamber. Placement of the heating elements is shown in chapter 3. The power P of the each heating element was chosen to be 100 W, to provide sufficient heating of the whole probe. For input voltage $U = 28\,\mathrm{V}$, the resistance of the wire is

$$R = \frac{U^2}{P} = \frac{28^2}{100} = 7.84\,\Omega.$$

The coils are switched by a circuit shown in figure 25. The mosfet transistor is used as a switch, which controls current flowing from input V_{in}, through the coil connected to a connector J_1, to the ground. The switched current is approximately 3.6 A. To prevent voltage spikes, the change of the control voltage HEATING_HEAD is slowed by an RC filter with time constant $\tau = 5\,\mu\mathrm{s}$. Resistor R_5 helps to keep the mosfet closed, when the control voltage equals zero. To prevent noise leaving/entering the pcb, 470 pF bypass capacitor is used.

To determine the temperature of the probe, NTC (negative temperature coefficient) thermistors are used. The schematic of the temperature-measuring circuit is shown in figure 26. The thermistor is connected to connector J2, in series with resistor R2. This creates a voltage divider. The change in resistivity of the thermistor will affect the voltage across its terminals. This voltage is measured by the adc, which is connected to TEMP_HEAD. For this application, I chose a thermistor with 5 kΩ resistivity at 25 °C. Another parameters of this part, including dependency of resistivity of the thermistor on its temperature, can be found in documentation [24]. From this documentation, R/T characteristic number 8016, we can determine the voltage U on terminals of the selected thermistor as

$$U = 5 \cdot \frac{R_T}{5100 + R_T},$$

where R_T is resistivity of the thermistor at temperature T. From the values of U and T, lookup table was created. This table will be used for determining temperature from the measured values of U. Additional calibration may be needed, however, to measure the temperature with desired accuracy.

The input to the ADC has 10 nF capacitor in a close vicinity for the reasons discussed in section 4.1.1. The 470 pF bypass capacitor is used to prevent noise leaving/entering

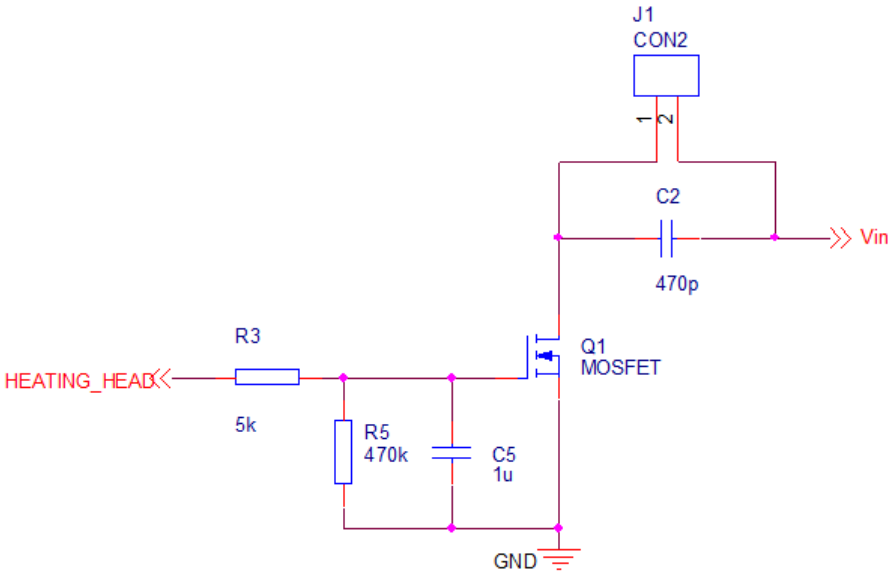

Figure 25 A schematic drawing of a heating switch circuit.

the pcb. The resistor R4 will not be assembled and provides surface for measuring probe.

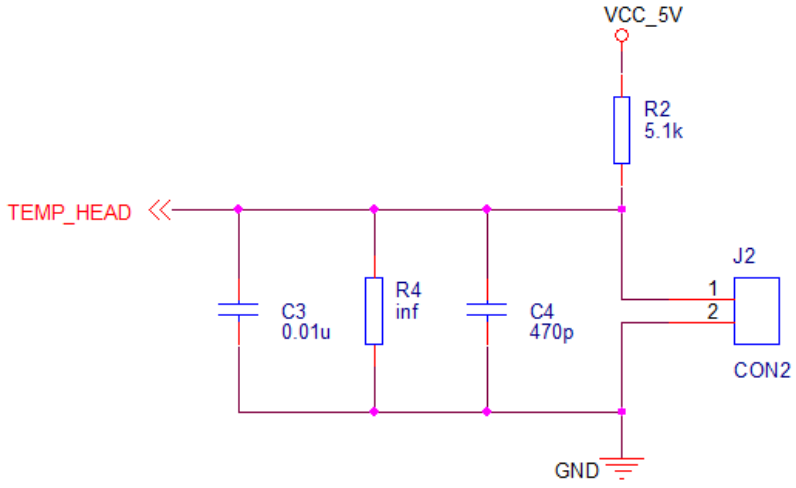

Figure 26 A schematic drawing of a thermistor circuit.

4.1.4 Interface

To communicate with the outside, the device contains RS232 and CAN transceiver.

RS232

The RS232 transceiver was chosen for its simplicity. Formerly, it was used for communication between computer and its peripherals. It contains one line driver and one receiver. For this application, a transceiver with extended temperature range of −55 °C to 125 °C was selected. The schematic drawing of the transceiver, created according to [25], is shown in figure 27.

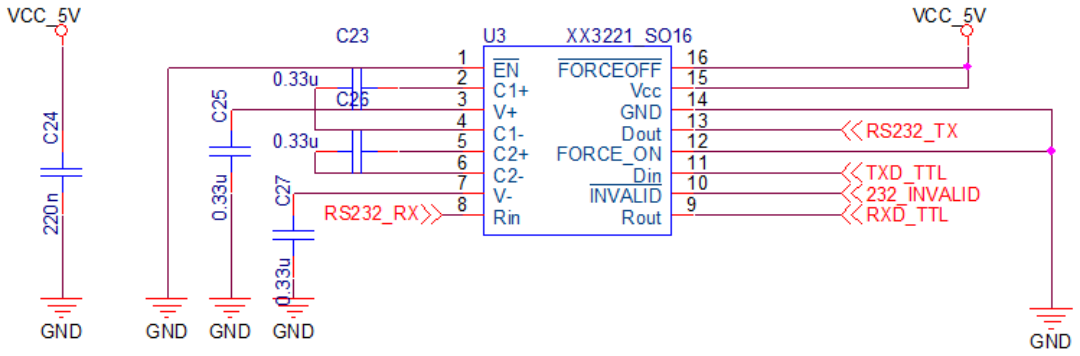

Figure 27 A schematic drawing of an RS232 transceiver circuit.

CAN

CAN bus was designed for automotive use, but it has spread into other sectors. The selected device has increased durability and is certified for use in automotive applications. The schematic drawing of the can transceiver created according to [25] is shown in figure 28.

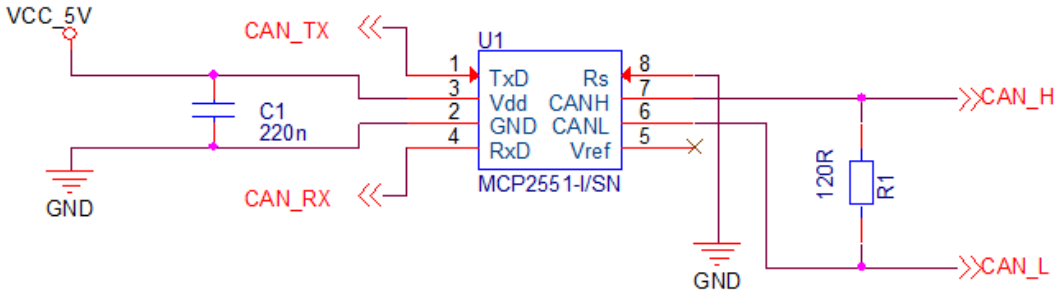

Figure 28 A schematic drawing of CAN circuit.

4.1.5 Microcontroller

This device is controlled by Freescale MC9S12XE microcontroller. Its main purpose is to convert analogous voltages from pressure sensors and thermistors to digital values, process them and transmit them by CAN or RS232. For signalling purposes, it uses open drain outputs described in section 4.1.6.

The schematic drawing of the microcontroller, shown in figure 33 in Appendix A, was created according to [18]. The microcontroller is programmed using a BDM connector. It contains LED for debugging purposes. If additional outputs are needed, connector CON6A is present.

4.1.6 Open drain output

Open drain outputs are used, when connecting environments with different voltage levels. Devices with higher or lower voltages can be connected.

When voltage is applied to the gate of the mosfet transistor, the drain is grounded, which can be used for example to turn on a light bulb or to switch a relay. This pcb contains three open drain outputs, which are intended for signalling. However, it can

also be used for another purpose. For this application, the open drain outputs can be used to indicate, that:

- heating is turned on
- aircraft is reaching critical angle of attack or sideslip
- device is malfunctioning

Schematic drawing of the used open drain circuit is shown in figure 29. To prevent very fast switching, the change of the gate voltage OPEN_DRAIN1 is slowed by an RC filter with time constant $\tau = 5\,\mu s$. Resistor R11 helps to keep the transistor closed. The mosfet transistor is made to withstand voltages up to 60 V, and currents up to 3 A.

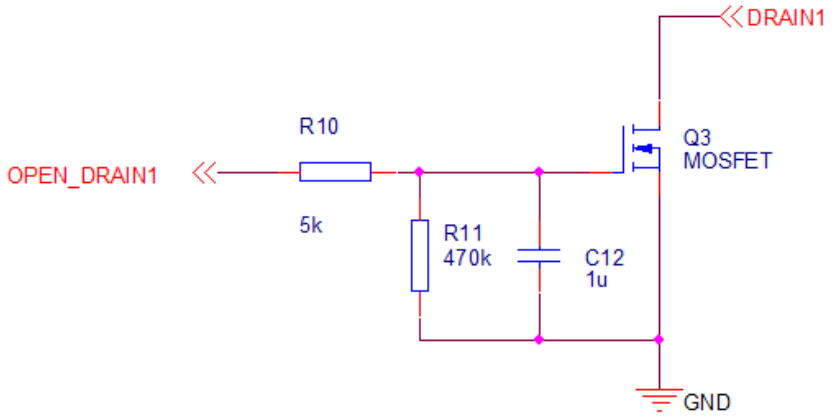

Figure 29 A schematic drawing of an open drain circuit.

4.1.7 D-Sub connector

All communication and power supply is provided through a single high-density D-Sub connector with 26 pins. The schematic drawing, from which the usage of individual pins can be seen, is shown in figure 34 in Appendix A. Most of the pins are used for power supply, to limit currents through individual lines. This should also decrease the inductance of the power supply. To prevent noise from entering or leaving the pcb through the power line, two 470 pF capacitors are situated nearby.

4.2 Printed circuit board design

In this section, I will be discussing the outcome of the pcb design process.

One of the goals of this work was to design a compact pcb, that would fit inside the vertical stem of the aerometric probe. The design was complicated by a few challenges. Most of the challenges were caused by the strongly elongated shape of the pcb. This made it difficult to apply the best practices of the pcb design. One of the best practices is to separate analogous, digital and power circuitry on the pcb. In my opinion, I accomplished this goal only partially. The respective parts are separated, but the distance are not always satisfactory. This was caused by the fact, that pressure sensors, thermistor connections and heating wire connections have to be situated near one side of the pcb—the narrow one. On the opposite side of the pcb, a single connector for all the data and power signals is placed. It would be better, if some of the signals had separate connectors, which would also made part placement easier.

At first, we decided to create a 2-layer board, which we thought would be sufficient. I managed to place all the components and route all the traces, but had to make some compromises. For example, power supply lines between the microcontroller and power supply, which should be as short as possible, had to be routed through multiple vias. Routing noisy signals—which microcontroller power supply is—through vias is generally considered a design flaw. As another example, power supply lines for pressure sensors had to be routed near oscillator circuit of the microcontroller, where high frequency coupling might occur. Overall grounding was also unsatisfactory.

After discussion with my supervisor, we decided to create a 4-layer pcb, which is shown in figure 31. Logical parts are highlighted. Cross section of the pcb is shown in figure 30 and the layers are stacked as follows:

1. Top
2. Ground
3. Power
4. Bottom

The usage of power distribution layers made routing easier, and a lot of design flaws were removed.

Figure 30 Cross section of a four layer pcb made by Pragoboard [26].

As we can see from figure 30, the two inner power distribution layers are spaced 1.2 mm apart, so this is a pcb with widely-spaced layers. This means, that the inductance between power distribution layers cannot be neglected. This has consequences for placement of decoupling capacitors—placing decoupling capacitors closely to the part being decoupled lowers the inductance of the connections, so the current is firstly drawn from the capacitor, before it is drawn from the power planes. Decoupling capacitors on pcb-s with layers spaced closely can be placed farther from the device, because the currents are drained firstly from the power layers, and decoupling capacitors act globally [27].

From the logical parts highlighted in figure 31, two needed increased attention: the switching power supply, and the microcontroller.

4.2.1 Layout of the switching power supply

A bad layout of the switching power supply could impact operation of the device, and other devices in the vicinity. For devices containing ATD converters it is especially important, that the supply voltage is stable. Switching power supplies are known for having ripple on the output voltage, which can be filtered out by multiple capacitors. To prevent excessive ripple on the input and output voltage, a ceramic capacitor C18 has to be placed as close as possible to the input of the regulator.

Another critical part is the power diode D3. The regulator contains an internal mosfet transistor, which periodically interrupts current flow through the regulator. When the current flow through the regulator is suddenly interrupted, the inductor tries to

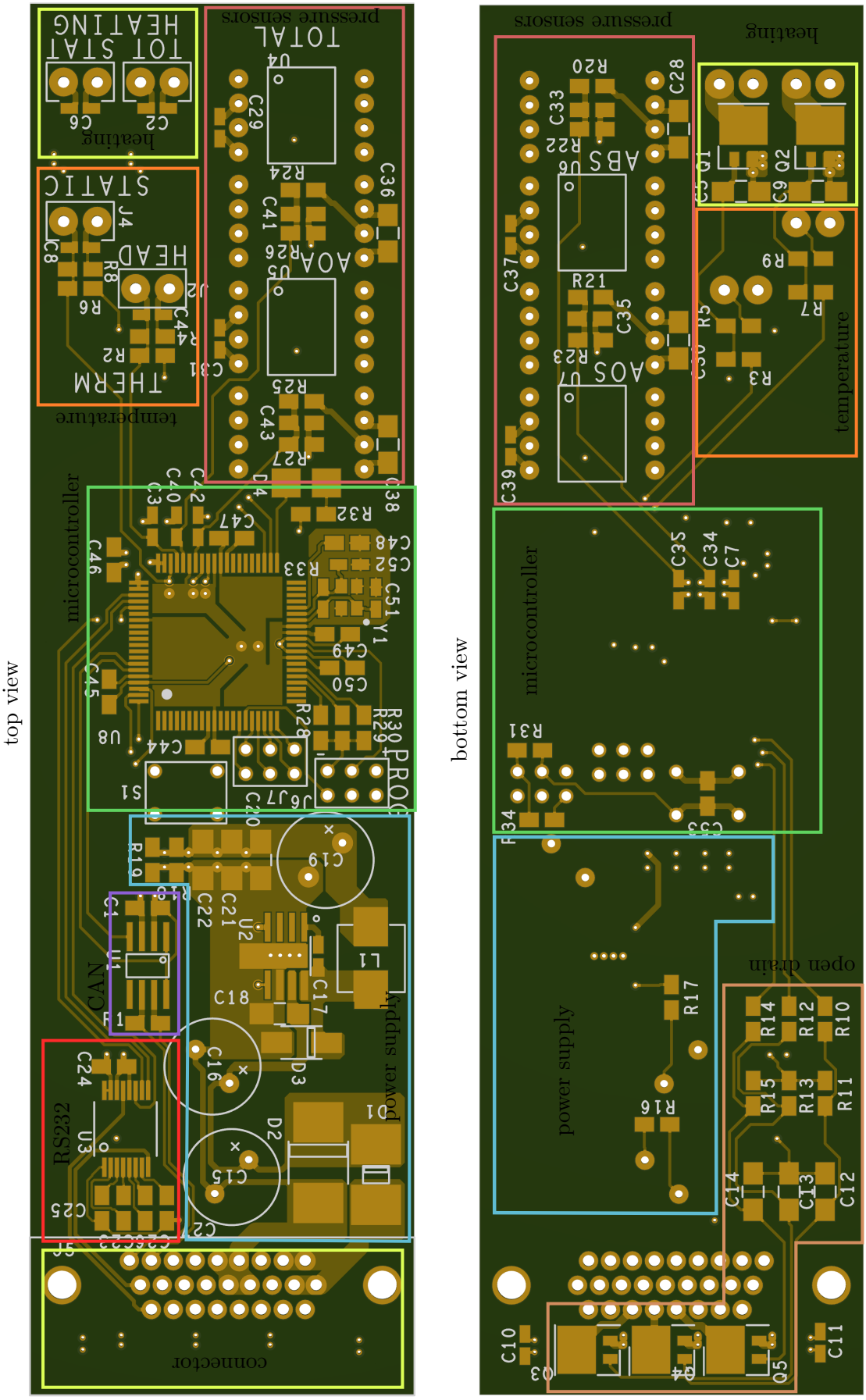

Figure 31 Top and bottom view of designed pcb.

maintain this current constant, which results in opening of the power diode D3 and changing of the current path. These changes in the current path create changing magnetic field, so it is desirable to minimize the differences between the two current paths and to keep the vicinity free of conducting surfaces, to prevent interference caused by induced currents.

To read the output voltage, the regulator has a feedback. The connection from the output to the feedback pin has to be routed away from noisy lines, so I situated it on the bottom side of the pcb, away from rapidly-changing currents of the regulator.

The area around regulator contains a lot of copper, to increase heat conductivity. I also added a few thermal vias right under the regulator, to draw heat to the inner ground layer [19][28][29].

4.2.2 Microcontroller layout

For the layout of the microcontroller, I used information in [18] and [30].

The microcontroller was oriented in such a way, so the ADC inputs are as close as possible to the pressure sensors and thermistor circuit. This orientation keeps the precise analogous circuitry, including reference voltage pins decoupled by capacitor C46, away from return currents of the microcontroller. Furthermore, this places noisy circuit of the oscillator Y1 away from anything sensitive.

Under the microcontroller, a microcontroller ground is placed. The microcontroller ground has cuts, which guide currents of the respective parts of the device away from each other. In the middle, the microcontroller ground is connected to the ground layer through two vias. The purpose of this layout is to contain any interference caused by the device to the microcontroller ground. With proper decoupling, this approach should minimise the influence of the microcontroller on the ground layer.

4.2.3 Power distribution layers

In this design, the two inner layers are reserved for power distribution. Copper on the ground layer fills the whole area, and has no cuts in itself. Arrangement of the power layer is shown in figure 32. The power layer contains two planes: one is for distribution of 5 V from the power regulator, the second one conducts heating current for the probe. The heating current also increases temperature of the pcb, which is beneficial

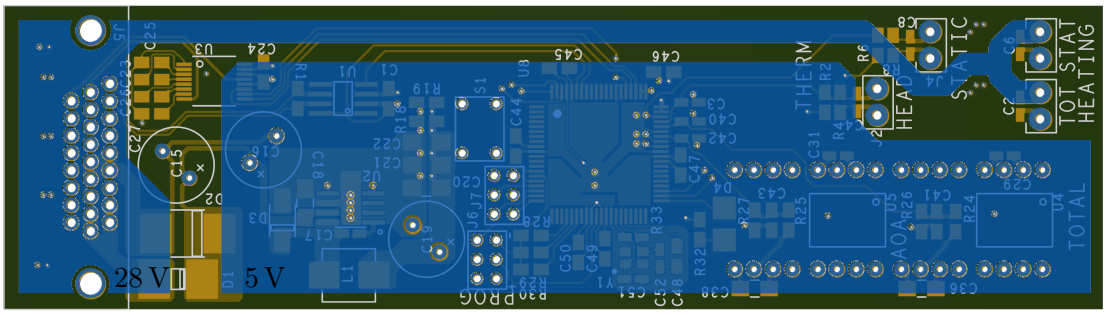

Figure 32 Inner power layer (blue) depicted over top side of the pcb.

Chapter 5

Conclusion

This thesis is focused on designing of a compact aerometric probe, which could be used on aircraft to measure airspeed, angle of attack, angle of sideslip and altitude. I propose a mechanical design of the probe, which is created in accordance with the currently available knowledge in this area. The probe is electrically heated, and contains means of removing water from the pressure ducts. The probe is controlled by a circuit board, which also provides measurement of the acquired pressures.

The aerometric probe, including circuit board, was manufactured and assembled according to the specifications described in this thesis.

For future work, I propose:

- To replace the plastic parts, which were made for testing purposes, by ones made of dural, to increase durability.
- The manufacturing of the heating element is rather complicated. It would be convenient to hire an external company to provide a solution according to our specifications.
- Encapsulating the circuit board in epoxy resin or silicone would be beneficial. It would add protection against moisture, mechanical or thermal shock, and also spread heat.
- The aerometric probe was not tested in a wind tunnel. It would be interesting to verify the quality of the design.

Appendix A

Tables and schematics

T (°C)	U (V)	T (°C)	U (V)
-55	4.948	45	1.499
-50	4.925	50	1.305
-45	4.894	55	1.132
-40	4.853	60	0.980
-35	4.798	65	0.848
-30	4.728	70	0.733
-25	4.637	75	0.634
-20	4.525	80	0.549
-15	4.387	85	0.476
-10	4.222	90	0.413
-5	4.029	95	0.359
0	3.810	100	0.313
5	3.567	105	0.273
10	3.306	110	0.239
15	3.032	115	0.209
20	2.752	120	0.184
25	2.475	125	0.162
30	2.207	130	0.143
35	1.952	135	0.127
40	1.715	140	0.113

Table 4 Lookup table for determination of the probe temperature.

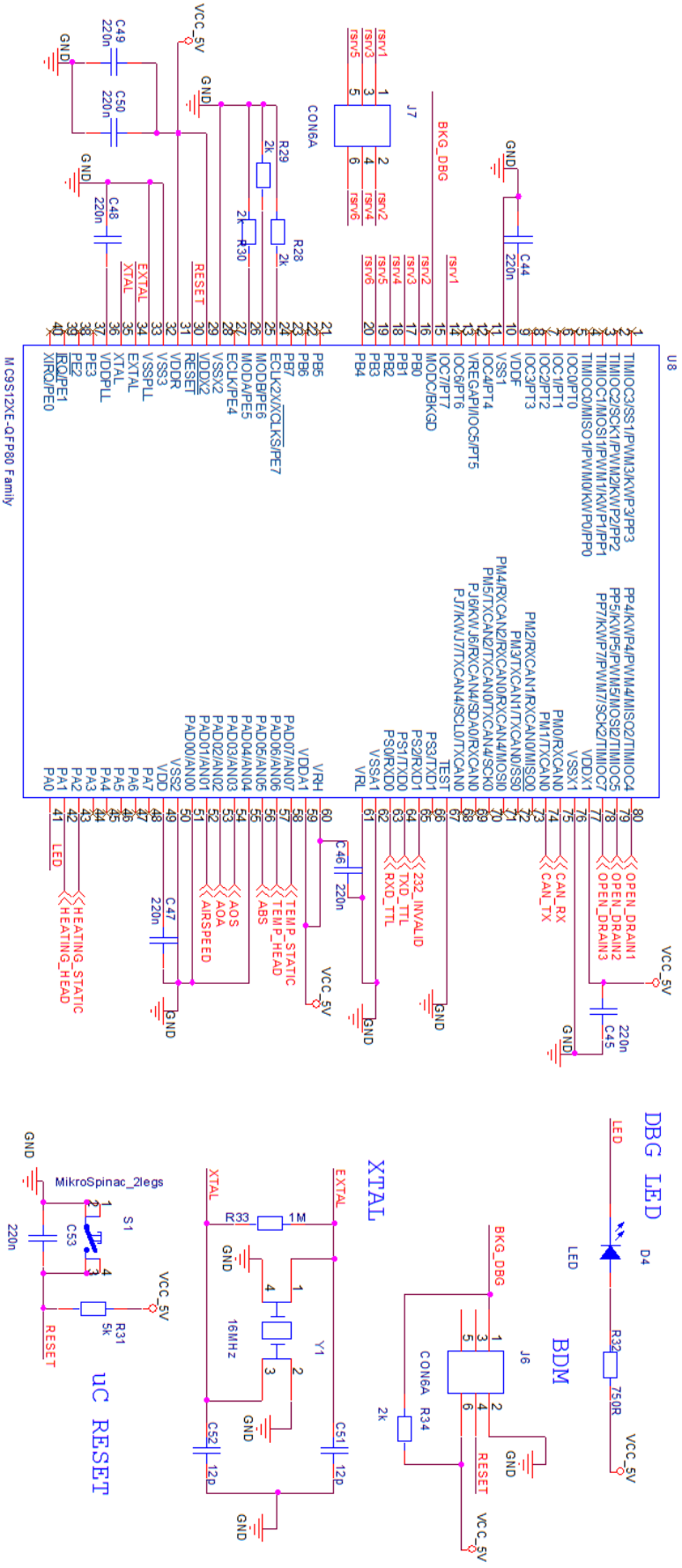

Figure 33 A schematic drawing of a microcontroller.

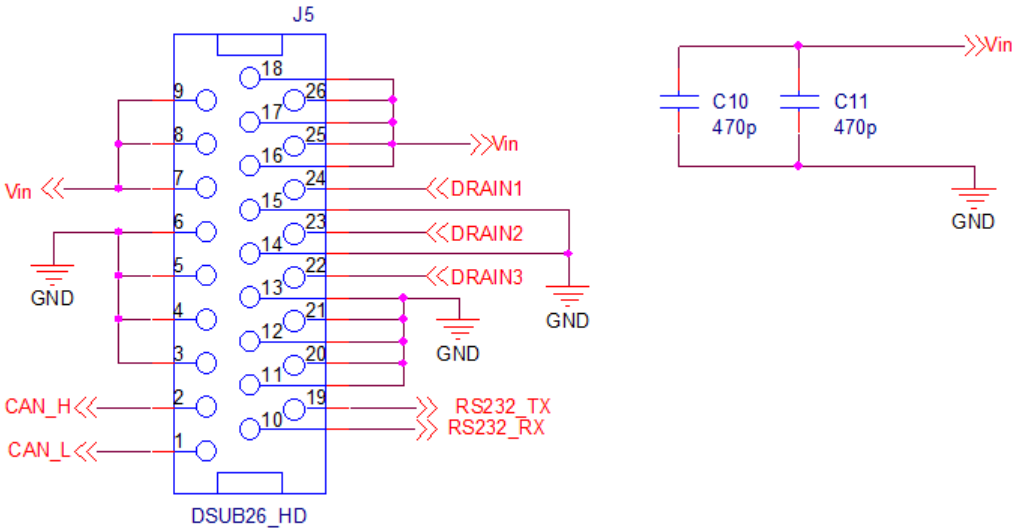

Figure 34 D-Sub connector.

Appendix B

CD content

The attached CD contains the following:

1. Text of this work
2. Files of the mechanical design
3. Files of the electronic design

Bibliography

[1] *State-of-the-Art Air Data Products*. URL: http://spaceagecontrol.com/Main/uploads/Main.Sitelist/s002a.pdf.

[2] William Gracey. *Summary of methods of measuring angle of attack on aircraft*. Tech. rep. National Advisory Committee for Aeronautics. Langley Aeronautical Lab.; Langley Field, VA, United States, 1958.

[3] P. Paces, J. Popelka, and J. Auersvald. "Standalone trailing probe for aero metrical measurements". In: *2012 IEEE/AIAA 31st Digital Avionics Systems Conference (DASC)*. Oct. 2012, DOI: 10.1109/DASC.2012.6382275.

[4] *Pitot-Static(Prandtl) Tube*. https://www.grc.nasa.gov/www/k-12/airplane/pitot.html.

[5] Federal Aviation Administration and Federal Aviation Administration/Aviation Supplies & Academics. *Instrument Flying Handbook: Faa-h-8083-15b*. FAA Handbooks. Aviation Supplies & Academics, 2013. ISBN: 9781619540569.

[6] B. Eckert. *Experiences with Flow-direction Instruments*. Tech. rep. National Advisory Committee for Aeronautics; Washington, DC, United States, 1941.

[7] Kenneth G Merriam and Ellis R Spaulding. *Comparative Tests of Pitot-static Tubes*. Tech. rep. National Advisory Committee for Aeronautics; Washington, DC, United States, 1935.

[8] William Gracey. *Wind-tunnel investigation of a number of total-pressure tubes at high angles of attack – subsonic, transonic, and supersonic speeds*. Tech. rep. National Advisory Committee for Aeronautics. Langley Aeronautical Lab.; Langley Field, VA, United States, 1957.

[9] Wilber B. Huston. *Accuracy of airspeed measurements and flight calibration procedures*. Tech. rep. National Advisory Committee for Aeronautics. Langley Aeronautical Lab.; Langley Field, VA, United States, 1948.

[10] K. Hilding Beij. *Aircraft Speed Instruments*. Tech. rep. National Advisory Committee for Aeronautics. Langley Aeronautical Lab.; Langley Field, VA, United States, 1933.

[11] W. F. Lindsey. *Calibrations of Service Pitot Tubes in the Langley 24-inch High-speed Tunnel*. Tech. rep. National Advisory Committee for Aeronautics. Langley Aeronautical Lab.; Langley Field, VA, United States, 1946.

[12] William Gracey. *Measurement of static pressure on aircraft*. Tech. rep. National Advisory Committee for Aeronautics. Langley Aeronautical Lab.; Langley Field, VA, United States, 1958.

[13] Virgil S. Ritchie. *Several Methods for Aerodynamic Reduction of Static-Pressure Sensing Errors for Aircraft at Subsonic, Near-Sonic, and Low Supersonic Speeds*. Tech. rep. National Aeronautics and Space Administration, Langley Station, Va. Langley Research Center, 1959.

[14] Roy E. Rayle. "An investigation of the influence of orifice geometry on static pressure measurements". Master's thesis. Massachusetts Institute of Technology. Dept. of Mechanical Engineering, 1949.

[15] *U.S. Standard Atmosphere, 1976*. Tech. rep. NASA; Washington, DC, United States National Oceanic and Atmospheric Administration; Department of the Air Force; Washington, DC, United States, 1976.

[16] A Reodique and W Schultz. *Noise Considerations for Integrated Pressure Sensors*. Tech. rep. Freescale Semiconductor, 2005.

[17] STMicroelectronics. *Understanding and minimising ADC conversion errors*. 2003.

[18] Freescale Semiconductor. *MC9S12XEP100 Reference Manual*. 2013. URL: http://www.nxp.com/assets/documents/data/en/data-sheets/MC9S12XEP100RMV1.pdf.

[19] Texas instruments. *LM22676/LM22676-Q1 42V, 3A SIMPLE SWITCHER® Step-Down Voltage Regulator with Features*. 2013.

[20] Vishay. *Aluminum Capacitors Radial, High Temperature, Low Impedance*. 2012.

[21] Vishay. *Aluminum Capacitors*. 2014.

[22] Vishay. *Surface Mount TRANSZORB® Transient Voltage Suppressors*. 2013.

[23] Vishay. *Transient Voltage Suppressors (TVS) for Automotive Electronic Protection*. 2010.

[24] EPCOS. *NTC thermistors for temperature measurement*. 2013.

[25] Texas Instruments. *MAX3221, 3-V to 5.5-V single channel RS232 driver/receiver with ±15-kV ESD protection*. 2006. URL: http://www.ti.com/lit/ds/symlink/max3221-ep.pdf.

[26] *POOL servis–princip výroby*. URL: http://www.pragoboard.cz/pool_servis.

[27] *Circuit Board Decoupling Information*. URL: http://learnemc.com/circuit-board-decoupling-information.

[28] ROHM Semiconductor. *PCB Layout Techniques of Buck Converter*. URL: http://rohmfs.rohm.com/en/products/databook/applinote/ic/power/switching_regulator/converter_pcb_layout_appli-e.pdf.

[29] Jeff Barrow. *Reducing Ground Bounce in DC-to-DC Converters–Some Grounding Essentials*. URL: http://www.analog.com/media/en/analog-dialogue/volume-41/number-2/articles/reducing-ground-bounce-in-dc-to-dc-converters.pdf.

[30] Gallop. Martyn. *Designing Hardware for the HCS12 D-Family*. Freescale Semiconductor. 2004. URL: http://www.nxp.com/assets/documents/data/en/application-notes/AN2727.pdf.